Physics – Uspekhi **51** (7) 727 – 748 (2008)

CONFERENCES AND SYMPOSIA PACS numbers: 01.10.Fv; 71.35.Ji, 73.20.Mf, **73.21. – b**; 72.80.Rj, **73.43. – f**, 81.05.Uw

Collective electron phenomena and electron transport in graphene (Scientific session of the Physical Sciences Division of the Russian Academy of Sciences, 27 February 2008)

Yu E Lozovik, S P Merkulova, A A Sokolik;
S V Morozov, K S Novoselov, A K Geim

DOI: 10.1070/PU2008v051n07ABEH006793

A scientific session of the Physical Sciences Division of the Russian Academy of Sciences (RAS) was held on February 27, 2008 in the conference hall of the Lebedev Physical Institute, RAS. The following reports were presented at the session:

(1) **Lozovik Yu E, Merkulova S P, Sokolik A A** (RAS Institute for Spectroscopy, Troitsk, Moscow Region) "Collective electron phenomena in graphene";

(2) **Morozov S V** (RAS Institute for Problems in Microelectronics Technology, Chernogolovka, Moscow Region), **Novoselov K S, Geim A K** (University of Manchester, Manchester, UK) "Electron transport in graphene."

An abridged version of these reports is given below.

PACS numbers: 71.35.Ji, 73.20.Mf, **73.21. – b**
DOI: 10.1070/PU2008v051n07ABEH006574

Collective electron phenomena in graphene

Yu E Lozovik, S P Merkulova, A A Sokolik

1. Introduction

Carbon is one of the most interesting chemical elements. It not only forms the basis of the vast kingdom of organic substances but itself forms various crystals and nanostructures. This plethora of forms stems from the ability of carbon atoms to connect to one another in different ways and to create very different lattices and chains.

As a result of hybridization of s- and p-orbitals of four valence electrons, a carbon atom can form covalent bonds with its neighbors, such that different ways of hybridization result in different orientations and different numbers of bonds.

In the case of sp^3 hybridization, carbon atoms join to form a three-dimensional system, the tetrahedral crystalline lattice of diamond, and the sp^2 hybridization results in a two-dimensional planar structure, the graphene, whose crystal lattice looks like a hexagonal honeycomb. The most conventional form of carbon — graphite — can be regarded as a stack of graphene sheets bound together relatively weakly by van der Waals forces.

Uspekhi Fizicheskikh Nauk **178** (7) 757 – 780 (2008)
DOI: 10.3367/UFNr.0178.200807g.0757
Translated by V I Kisin; edited by A M Semikhatov

Carbon also forms quasi-one-dimensional structures — carbon nanotubes whose different types can be regarded as graphene sheets rolled into tubes in various ways (see, e.g., reviews [1]). A quasi-zero-dimensional carbon nanostructure — a fullerene — can be considered to result from 'tiling' a sphere by a 'honeycomb'-type graphene lattice. By virtue of Euler's theorem, at least 12 'defects' need to be introduced into this lattice; their role is played by pentagonal cells (see, e.g., [2]). In some sense, therefore, graphene is a key quasi-two-dimensional system, which generates quite diverse structures from the viewpoint of classification: three-dimensional graphite, quasi-one-dimensional nanotubes, and quasi-zero-dimensional fullerenes.

The weak coupling and relative independence of graphene layers in graphite crystals (the property that is used in ordinary pencils) were a hint to researchers that graphene could be prepared as an isolated object, a membrane one atom thick [3]. In addition to the inevitable technical complications, there were certain doubts that graphene as a two-dimensional planar structure could be stable at all. As followed from Peierls's and Landau's arguments [4], logarithmic divergence of long-wave fluctuations of atomic two-dimensional displacements from lattice sites made long-range order impossible in a purely two-dimensional system. However, it became clear after the classic results of Berezinskii [5] and Kosterlitz and Thouless [6] that although there is no crystalline ordering in a two-dimensional system, a quasi-long-range power-law order exists in the low-temperature phase; this order preserves the principal property of the crystal, the long-wavelength shear modulus (it disappears upon melting, which occurs as a phase transition that uncouples pairs of dislocations [7]). The statements above are strictly valid for ordering in a purely two-dimensional system, and doubt stemmed from something different: is an isolated graphene sheet stable as a two-dimensional membrane in three-dimensional space — in other words, would displacement fluctuations perpendicular to the sheet transform graphene into a crumpled ball?

The new era for graphene started in 2004, when it was prepared by Novoselov, Geim, Morozov, et al. [8, 9] using micromechanical graphite cleavage. In this method, the surface of graphite is tightly rubbed on a smooth surface of silicon covered with a layer of oxide, on which it leaves numerous flakes of different thicknesses. The silicon oxide surface was chosen because flakes of even monatomic thickness can be viewed on it with an optical microscope. In their first experiments, Novoselov, Geim, Morozov, et al. obtained specimens of one-, two-, and multilayer graphene

and studied their transport properties [10]. Graphene was found to be stable in air at room temperature. It is mechanically stable on a substrate, although small local curved nanosized patches — 'ripples' — are formed on it [11].

Graphene preparation by micromechanical techniques proved to be a fairly cumbersome process, because every sufficiently thin flake had to be investigated by an atomic force microscope in order to ascertain that it indeed had a monatomic thickness. It was later shown, however, that the number of graphene layers in a specimen can be readily determined, e.g., by studying the spectrum of Raman scattering [12]. We also mention the invention of an alternative, now widely used method of graphene preparation — epitaxial growth [13], in which graphene layers are formed on the surface of an SiC crystal heated in a vacuum to a high temperature.

The news of graphene preparation created quite a stir and reached a high pitch after the unique properties of this system were experimentally discovered. From the standpoint of applications, graphene is interesting, first of all, as a material for building nanoelectronic devices. Being a two-dimensional system, graphene provides the absolute limit of miniaturization, at least in one dimension, and ideally suits today's planar technologies of building integrated circuits. Using nanolithography, arbitrarily shaped pieces can be cut out of graphene, and contact or contactless electrodes can be mounted on them [14]. Furthermore, various structures with a periodic superlattice that may have interesting properties can be created using a graphene sheet as the base (e.g., by depositing an ordered layer of adatoms [15] or by making periodically spaced orifices [16]). The mobility of charge carriers in pure graphene specimens has reached record high values [17] and is almost independent of concentration, which is also a valuable property for potential applications (including ballistic electronics, which differs in principle from the traditional transistor electronics). We note that the gap between Landau levels in graphene in the typical laboratory magnetic fields 10 – 20 T reaches several thousand degrees, which allows observing the quantum Hall effect and using it for designing resistance standards operating even at room temperature [18].

Graphene is interesting not only in view of possible applications but also from the fundamental standpoint, in view of its unique electron properties. Electrons in graphene close to the Fermi level have linear dispersion and the energy gap between the valence and conduction bands is zero, and hence electrons can be described by the two-dimensional Dirac equation for massless particles. This remarkable fact was established 60 years ago in the classic paper by Wallace [19]. The wonderful poet Rainer Maria Rilke was perhaps right when he said that whatever our mind draws from memory will some day turn into a blessing. The model of the graphene band structure has served as a launching pad for studying the properties of graphite, but the interaction between layers in multilayer stacks significantly changes the properties of graphene. Only after 2004, after it was possible to isolate individual graphene sheets, did it become clear that this system actually allowed studying a new type of particle — charged massless quasiparticles that do not exist anywhere else in nature [20]. The properties of these particles such as two-dimensionality, a spinor nature, and zero mass and zero gap in the spectrum give rise to a number of electron phenomena that have no analogs in any other physical system.

We begin with a brief review of the main features of the one-particle (Sections 1 – 3) and collective (Section 4) properties of graphene (see also review papers [21 – 23]) and then present our original results concerning certain collective electron phenomena (Sections 5 – 9). In the concluding part, Section 10, we discuss the fundamental problems of graphene physics and prospects for its future uses.

2. The Dirac equation for electrons in graphene

Each carbon atom in graphene is surrounded by three nearest neighbors and has four valence electrons. Three electrons form sp^2 hybridized orbitals at 120° to one another that constitute covalent bonds with neighboring atoms oriented in the same plane. The fourth electron, represented by a $2p_z$ orbital oriented perpendicularly to this plane, can hop from one atom to another and forms a half-filled π band responsible for electron properties of graphene (Fig. 1).

The theoretical analysis of electron properties of graphite started by considering the band structure of its elementary block, graphene. This was first considered by Wallace in 1947. In the simple tight-binding approximation with the interaction with the nearest neighbors taken into account, Wallace was able to show [19] that the dispersion of graphene electrons close to the Fermi level is linear and there is no gap. It was shown later that the linear nature of dispersion follows from the symmetry group of the graphene crystal lattice, regardless of the approximation used [24]. The band theory of graphene was subsequently improved and detailed [25, 26], but in connection with experimental studies of intercalated graphite [27] interest was stimulated in some of the multiparticle aspects of the electron properties of graphene (such as impurity screening [28], plasmons [29], and quasiparticle lifetimes [30]). Furthermore, interesting papers appeared on the effects of disorder [31] and on Landau levels in a magnetic field in graphene [32].

We now outline the main points of the band theory of graphene [19, 24, 33] that led to the conclusion that the effective equation for electrons in graphene is indeed the Dirac equation for massless particles. The graphene crystal lattice — the 'hexagonal honeycomb' — can be presented as a combination of two interpenetrating Bravais lattices A and B, with the unit cell forming a parallelogram (Fig. 2). The period

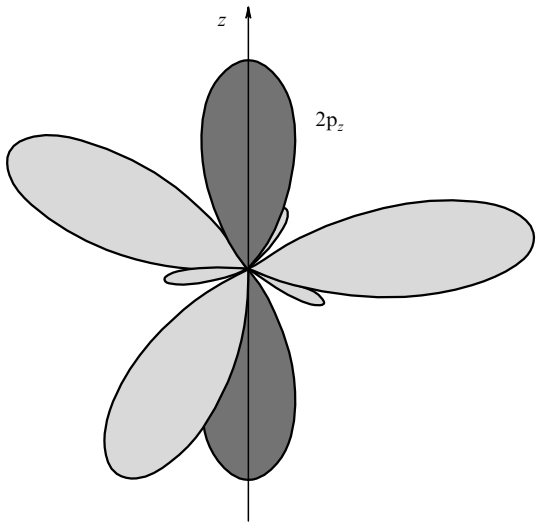

Figure 1. Three sp^2 hybridized orbitals of the carbon atom at 120° to one another, forming covalent bonds with neighboring atoms and a $2p_z$ orbital perpendicular to them.

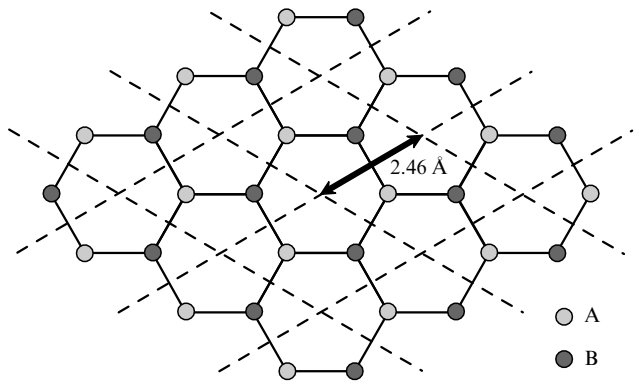

Figure 2. Two-dimensional honeycomb-type crystal lattice of graphene as a combination of two interpenetrating sublattices A and B.

of these lattices is $a = 2.46$ Å and their first Brillouin zone is a hexagon with the side $4\pi/3a$. Since the periodic potential of the lattice is created by two sublattices shifted relative to one another, the wave function of the electron in this potential is a linear combination of two Bloch waves built on these sublattices:

$$\psi(\mathbf{r}) = \psi_{\mathrm{A}}(\mathbf{r})\, X_{\mathrm{A}}(\mathbf{k},\mathbf{r}) + \psi_{\mathrm{B}}(\mathbf{r})\, X_{\mathrm{B}}(\mathbf{k},\mathbf{r})\,, \tag{1}$$

where $\mathbf{k}$ is the quasimomentum of the electron. The expansion coefficients ψ_j ($j = \mathrm{A}, \mathrm{B}$) are envelopes of the Bloch waves and play the role of the effective electron function that obeys the effective equation — an analog of the 'effective mass' approximation. Because there are two such envelopes in the case of graphene, the effective wave function of the electron is two-component.

Wave function (1) must satisfy the Schrödinger equation

$$\left[-\frac{\hbar^2\nabla^2}{2m_{\mathrm{e}}} + U(\mathbf{r}) - E\right]\psi(\mathbf{r}) = 0\,, \tag{2}$$

where $U(\mathbf{r})$ is a periodic potential. The operator of kinetic energy results in a number of terms in which the differentiation operator ∇ acts on the functions $\psi_j(\mathbf{r})$ and $X_j(\mathbf{k},\mathbf{r})$. An important role in the subsequent analysis is played by the **kp**-approximation [25] in which the effective equation for the envelopes is derived under the assumption that the electron quasimomentum lies in the neighborhood of the selected point $\mathbf{K}$ of the Brillouin zone. Strictly speaking, the dependence of the envelopes on the coordinate ψ_j already suggests that the electron no longer has a definite quasimomentum (e.g., if it is in an external field). But the **kp**-approximation assumes that the uncertainty in the quasimomentum is small compared with the size of the Brillouin zone (the vector of the reciprocal lattice) or, in other words, envelopes change insignificantly on the scale of the lattice constant. This allows neglecting terms of the form $X_j(\nabla^2\psi_j)$ because they are small in comparison with the other terms, and setting the quasimomentum in formula (1) equal to $\mathbf{K}$. This results in the equation

$$\sum_{j=\mathrm{A},\mathrm{B}}\left\{\psi_j(\mathbf{r})\left[-\frac{\hbar^2\nabla^2}{2m_{\mathrm{e}}} + U(\mathbf{r}) - E\right]X_j(\mathbf{K},\mathbf{r}) + \frac{1}{m_{\mathrm{e}}}\{-\mathrm{i}\hbar\nabla X_j(\mathbf{K},\mathbf{r})\}\{-\mathrm{i}\hbar\nabla\psi_j(\mathbf{r})\}\right\} = 0\,. \tag{3}$$

We multiply (3) from the left first by $X_{\mathrm{A}}^*(\mathbf{K},\mathbf{r})$ and then by $X_{\mathrm{B}}^*(\mathbf{K},\mathbf{r})$, and each time integrate with respect to $\mathbf{r}$ over a region much larger than the lattice constant but such that the envelopes do not yet change significantly within it. We take into account that the expression in brackets in (3) 'sandwiched' between the functions X_k and X_j yields $\delta_{jk}(E_{\mathbf{K}} - E)$ after integration, where $E_{\mathbf{K}}$ is the energy of the electron with the quasimomentum $\mathbf{K}$. This gives two equations for $k = \mathrm{A}, \mathrm{B}$:

$$\sum_{j=\mathrm{A},\mathrm{B}}\left\{-\frac{\mathrm{i}\hbar}{m_{\mathrm{e}}}\langle X_k|\nabla|X_j\rangle(-\mathrm{i}\hbar\nabla) + \delta_{jk}(E_{\mathbf{K}} - E)\right\}\psi_j = 0\,. \tag{4}$$

As noted above, the first Brillouin zone of graphene is a hexagon. In undoped graphene, electrons with quasimomenta at the hexagon vertexes have the Fermi energy [19]. Hence, to allow expansion in the vicinity of the Fermi energy, $\mathbf{K}$ has to be chosen in the vertexes of the hexagon. It is readily shown by restructuring the Brillouin zone [24] that the Fermi surface in undoped graphene degenerates into two nonequivalent points (Dirac points) that entirely belong to the first Brillouin zone, and therefore it is sufficient to select any two vertexes of the hexagon to describe the states of the electron (Fig. 3). The presence of two valleys $\mathbf{K}$ and $\mathbf{K}'$ of the conduction band effectively doubles the number of fermions in graphene (two 'flavors' of electrons).

The diagonal matrix elements of momentum $\langle X_j|\nabla|X_j\rangle$ are zero. The nondiagonal elements are most simply calculated in the nearest-neighbor approximation when hops between $2\mathrm{p}_z$ orbitals of only the nearest atoms of the neighbor sublattices are taken into account. We then obtain

$$\langle X_{\mathrm{A}}| - \mathrm{i}\hbar\nabla|X_{\mathrm{B}}\rangle = \langle X_{\mathrm{B}}| - \mathrm{i}\hbar\nabla|X_{\mathrm{A}}\rangle^* \propto \mathbf{e}_x - \mathrm{i}\mathbf{e}_y\,.$$

As a result, set of equations (4) is now written as

$$-\mathrm{i}\hbar v_{\mathrm{F}}\begin{pmatrix} 0 & \dfrac{\partial}{\partial x} - \mathrm{i}\dfrac{\partial}{\partial y} \\ \dfrac{\partial}{\partial x} + \mathrm{i}\dfrac{\partial}{\partial y} & 0 \end{pmatrix}\begin{pmatrix}\psi_{\mathrm{A}}\\ \psi_{\mathrm{B}}\end{pmatrix} = E\begin{pmatrix}\psi_{\mathrm{A}}\\ \psi_{\mathrm{B}}\end{pmatrix},$$

or, in a compact form, as an equation for a two-component spinor ψ:

$$v_{\mathrm{F}}(\boldsymbol{\sigma}\mathbf{p})\,\psi = E\psi\,. \tag{5}$$

Here, $v_{\mathrm{F}} \approx 10^6$ cm s^{-1} is the speed of electrons on the Fermi surface determined by the lattice parameters, and $\boldsymbol{\sigma} = \{\sigma_x, \sigma_y\}$ is a two-dimensional vector of Pauli matrices. If an electron is in an external potential $V(\mathbf{r})$ that varies smoothly over distances of the order of the lattice constant, it enters equation (5) as an addition (diagonal in the sublattices) to the kinetic energy $v_{\mathrm{F}}(\boldsymbol{\sigma}\mathbf{p})$.

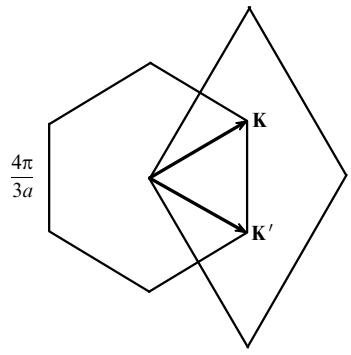

Figure 3. The first Brillouin zone of graphene in two equivalent representations: as a hexagon and as a rhombus. The two Dirac points lie entirely within this zone.

If the potential changes abruptly in space and therefore affects each sublattice in a different way, Eqn (5) acquires terms nondiagonal in the sublattices. When an electron is in a smoothly varying external magnetic field, the field enters Eqn (5) in a standard gauge-invariant manner, through the minimal substitution $\mathbf{p} \to \mathbf{p} + (e/c)\,\mathbf{A}$.

Equation (5) gives a dispersion relation for free particles $E = \pm v_{\mathrm{F}}|\mathbf{p}|$, which is typical of particles with zero mass. To establish a more thorough analogy with Dirac – Weyl equations that describe neutrinos [34], we recall that there are two valleys of the conduction band. The equation for two spinors $\psi_{\mathbf{K}}$ and $\psi_{\mathbf{K}'}$ corresponding to electrons in different valleys are written as $v_{\mathrm{F}}(\boldsymbol{\sigma}\mathbf{p})\,\psi_{\mathbf{K}} = E\psi_{\mathbf{K}}$ and $-v_{\mathrm{F}}(\boldsymbol{\sigma}\mathbf{p})\,\psi_{\mathbf{K}'} = E\psi_{\mathbf{K}'}$ (the change of the sign of the kinetic energy reduces to a gauge transformation). By combining $\psi_{\mathbf{K}}$ and $\psi_{\mathbf{K}'}$ into a four-component bispinor ψ, we arrive at the Dirac equation for a massless particle [1]:

$$p_\mu \gamma^\mu \psi = 0, \quad \mu = 0, 1, 2, \tag{6}$$

with the 'covariant' momentum $p_\mu = \{E/v_{\mathrm{F}}, -\mathbf{p}\}$ and gamma matrices

$$\gamma^0 = \begin{pmatrix} 0 & I \\ I & 0 \end{pmatrix}, \quad \gamma^{1,2,3} = \begin{pmatrix} 0 & \sigma_{x,y,z} \\ -\sigma_{x,y,z} & 0 \end{pmatrix}.$$

By analogy with quantum electrodynamics, we can introduce the chirality operator [36]

$$\gamma^5 = \mathrm{i}\gamma^0\gamma^1\gamma^2\gamma^3 = \begin{pmatrix} -I & 0 \\ 0 & I \end{pmatrix}.$$

Hence, electrons from different valleys correspond to states with opposite chiralities. If the mass is zero, states with opposite chiralities are independent; a nonzero mass would result in mixing them.

It must be remembered that the equation for electrons in graphene differs from the relativistic equations for massless fermions in several important respects:

1) the equation for electrons in graphene is two-dimensional;

2) representation (6) only holds at low momenta, much smaller than the reciprocal lattice vector and correspondingly only in smoothly varying external fields;

3) equation (6) holds in the lattice-at-rest reference frame and is not invariant under either Galilei or Lorentz transformations.

This last point calls for some clarification. The effective equation for electrons in graphene is derived from nonrelativistic Schrödinger equation (2), which is invariant under Galilei transformations (and hence describes *nonrelativistic* electrons). This invariance is lost in the derivation of effective equation (6) just as it is lost in deriving any 'effective mass' equation [37]. As regards the Lorentz transformations, the transition to a moving reference frame transforms the coordinate vector x^μ by a formula that includes the speed of light c. The speed of light also enters the gauge-invariant substitution $\mathbf{p} \to \mathbf{p} + (e/c)\,\mathbf{A}$ in (6), which is required for describing graphene in a magnetic field. At the same time, the spatial and temporal components of the momentum vector p_μ are related via the Fermi velocity $v_{\mathrm{F}} \approx c/300$. This mismatch of velocities destroys relativistic invariance.

[1] We note that the Dirac equation for massive particles was widely used for descriptions of narrow-band semiconductors (see [35] and the references therein).

3. Peculiarities of relativistic dynamics

The first experimental studies on graphene already confirmed that electrons behave as massless Dirac particles [10]. Data of the Shubnikov – de Haas oscillations showed that the electron dispersion is indeed linear and that the measured electron velocity v_{F} agrees with the calculations in the framework of the energy-band model. The anomalous integral quantum Hall effect discovered in graphene was a more spectacular feature. The energies of relativistic Landau levels of graphene in a strong magnetic field H are $E_{\pm n} = \pm\hbar v_{\mathrm{F}}\sqrt{2neH/(\hbar c)}$ [32]. An important factor is the zero energy level $n = 0$, of which one half belongs to the valence band and the other half to the conduction band. As a result of this peculiarity of the $n = 0$ level, the Hall conductivity of a graphene sheet in the quantum Hall regime assumes half-integral values in units of the conductivity quantum [38] $\sigma_{xy} = (4e^2/h)(n + 1/2)$, where n is an integer and the factor 4 corresponds to degeneracy in spin and valleys. This sequence of Hall plateaus discovered in experiment [10] was conclusive evidence of the 'ultrarelativistic' nature of electrons in graphene.

The band structure of graphene was also studied in the most straightforward way, by angle-resolved photoemission spectroscopy, which allows establishing the distribution of electrons in the momentum – energy space [39]. This investigation showed that although the dispersion close to the Dirac point is approximately linear, the interaction may distort it considerably. If graphene is strongly doped, the electron – electron, electron – phonon, and electron – plasmon interactions result in kinks on the dispersion curve at energies about 1 eV [40, 41].

The technique of controlling the charge concentration in graphene with an electric field [8] proved very convenient in its study. Graphene obtained by mechanical cleavage of graphite is placed on an oxidized silicon substrate covered by a layer of SiO_2, $d = 300$ nm thick. A voltage V_{g} between the graphene sheet and the substrate creates a capacitor with the capacitance per unit area $C/S = \varepsilon/(4\pi d)$, where $\varepsilon \approx 4.5$ is the dielectric permittivity of SiO_2. The surface charge density on the plates of such a capacitor is

$$n = \frac{CV_{\mathrm{g}}}{eS} = \frac{\varepsilon}{4\pi e d}\,V_{\mathrm{g}}. \tag{7}$$

By applying voltage of different polarity, it is possible to dope graphene with either electrons or holes. This controlling of the type of charge carriers and their concentration is very important from the standpoint of nanoelectronic applications. Furthermore, it is also important from the theoretical standpoint, because the ground state of doped graphene differs from the vacuum state as it is commonly understood in quantum electrodynamics. In the case of graphene, we can in some sense 'restructure' the vacuum.

We consider the free electron states in graphene; they serve as starting points for solving multiparticle problems. The eigenvector satisfying Eqn (5) and corresponding to the electron with a momentum $\mathbf{p}$ has the form $\psi_{\mathbf{p}}(\mathbf{r}) = \exp(\mathrm{i}\mathbf{p}\mathbf{r}/\hbar)\,f_{\mathbf{p},\gamma}$, which represents a plane wave times a spinor,

$$f_{\mathbf{p},\gamma} = \frac{1}{\sqrt{2}}\begin{pmatrix} \exp\left(-\dfrac{\mathrm{i}}{2}\,\varphi_{\mathbf{p}}\right) \\ \gamma\exp\left(\dfrac{\mathrm{i}}{2}\,\varphi_{\mathbf{p}}\right) \end{pmatrix}. \tag{8}$$

Here, $\gamma = \pm 1$ is the index of the band in which the electron is located; if $\gamma = 1$, then the electron with the energy $E = v_F|\mathbf{p}|$ is in the conduction band and if $\gamma = -1$, then it is in the valence band and its energy is $E = -v_F|\mathbf{p}|$. Expression (8) is an explicit function of γ and of the azimuthal angle $\varphi_{\mathbf{p}}$ of momentum. This angular dependence of the vectors of one-particle states is an important feature of graphene. It manifests itself in all expressions that describe transitions of electrons from one state to another. The transition amplitudes $|\mathbf{p}, \gamma\rangle \to |\mathbf{p}', \gamma'\rangle$ are multiplied by expressions of the type $f^{+}_{\mathbf{p}',\gamma'} f_{\mathbf{p},\gamma}$ that depend on the angle between the vectors $\mathbf{p}$ and $\mathbf{p}'$.

The spinor nature of electrons in graphene also manifests itself in that their Berry phase is equal to π: an electron following a closed path in the momentum space enclosing one of the two Dirac points changes the sign of its wave function. Indeed, expression (8) changes sign when the vector $\mathbf{p}$ rotates through 360°. In particular, the presence of $n = 0$ Landau levels ('zero modes') can be interpreted as a manifestation of the Berry phase [20]. The Berry phase is seen especially clearly in the effect of weak localization of electrons in random fields. Indeed, weak localization arises in ordinary two-dimensional systems as a result of constructive interference of amplitudes of electron waves scattered by impurities and moving in opposite directions along closed paths. In the case of graphene, the Berry phase causes an additional phase shift by π between the amplitudes of these waves, which transforms their constructive interference into a destructive one, resulting not in a weak localization but in an opposite effect, a weak antilocalization [42]. However, factors such as scattering by ripples and specimen edges and the disruption of spectrum isotropy at high momenta destroy the Berry phase. Consequently, weak localization and weak antilocalization compete in real graphene specimens [43].

The analogy between the dynamics of electrons in graphene and quantum electrodynamics gives hope that quantum-electrodynamic effects such as, for example, the Klein paradox will also be detected in graphene [44, 45]. This paradox manifests itself in electrons allowed to tunnel with high probability through a potential barrier whose height is larger than $2m_e c^2$, which is related to the contribution of the 'lower' underbarrier continuum. The creation of such barriers in quantum electrodynamics involves the presence of very strong electric fields, and hence the Klein paradox could be felt only in exotic situations (in collisions of superheavy nuclei, in the evaporation of black holes, etc.). In graphene, the effective mass is zero and therefore the Klein paradox should be detectable in tunneling through any barrier. A simple calculation shows [44] that for normal incidence on a potential step, the probability of transmission for an electron is strictly unity. That there is no backscattering in graphene has been known for quite some time in nanotubes; this is directly connected with the Berry phase [46]. This absence of backscattering can also be explained in terms of conservation of the 'pseudohelicity' $(\boldsymbol{\sigma}\mathbf{p})/|\mathbf{p}|$ in smoothly varying external fields — the projection of the electron momentum on its 'pseudospin' emerging due to the presence of two sublattices in graphene [44]. When an electron wave is incident on a one-dimensional potential barrier, the probability of wave transmission may reach unity at certain values of the incidence angle different from the normal incidence conditions.

The transparency of barriers, at least at certain incidence angles, results in the absence of strong localization under the conditions of applicability of the Dirac equation for envelopes [47]. This means that in a smoothly varying external field, an electron in graphene can form only quasi-bound states with a finite lifetime [48]. Conversely, bound states can be formed on 'pointlike' objects such as lattice defects [49]. Furthermore, the lifetime of quasi-bound states may be considerably increased by applying an additional magnetic field [50].

Klein tunneling can be used as a qualitative explanation of the emergence of a minimum in the conductivity of graphene [10, 51], which is not found in other quasi-two-dimensional systems. The conductivity of doped graphene is proportional to the concentration of electrons or holes, but when charge carrier concentration (7) passes through zero, the conductivity does not decrease below the universal nonzero value $4e^2/h$. The conductivity of even 'dirty' graphene never decreases below this value, which may be connected with the absence of localization for ultrarelativistic electrons.

Another analog of a quantum electrodynamic effect that can be studied in graphene is the spontaneous creation of electron–positron pairs around a supercritical charge. In quantum electrodynamics, the critical charge of the atom at which the energy level of the ground state belongs to the 'lower' continuum is $Z \approx 170$ [52]. However, according to some estimates, $Z = 2$ is already supercritical in graphene. Unusual resonance electron states must arise in the neighborhood of such a charge, and charge screening must also display anomalous features [53, 54].

In addition to single-layer graphene, experiments have produced specimens consisting of several layers [10]. The most interesting among them are two-layer graphene specimens for which the effective low-energy Hamiltonian is written as [55]

$$H = \frac{1}{2m^*} \begin{pmatrix} 0 & (p_x - \mathrm{i}p_y)^2 \\ (p_x + \mathrm{i}p_y)^2 & 0 \end{pmatrix}, \tag{9}$$

where $m^* = 0.033 m_e$. Electrons with this Hamiltonian have the Berry phase 2π, which reveals itself in an unusual form of the quantum Hall effect [56] and in specific features of Klein tunneling: normal incidence on a potential step in two-layer graphene produces total reflection, but incidence at certain angles results in transmission with probability one, as in one-layer graphene [44].

The dispersion law in two-layer graphene has the form $E = \pm p^2/2m^*$, which corresponds to two parabolic bands that touch each other. Such 'massive chiral fermions' do not exist in the traditional quantum field theory and constitute a unique feature of two-layer graphene. The possibility of creating a controlled gap in the spectrum of two-layer graphene under the application of a potential difference between two layers [57] is interesting and promising. The crystal band structure is usually fixed quite rigidly and is very stable under external influences, and hence the chance of controlling the gap width appears rather attractive from the standpoint of potential applications [58].

4. Peculiarities of collective phenomena in graphene

The characteristic features of the band structure of graphene — a linear dispersion and the bands touching at the Dirac point — are responsible for its unusual electron properties. If graphene is doped with a low concentration of Dirac electrons or holes, they interact both among themselves and with the filled valence band. The valence band is strongly

coupled to the conduction band because by virtue of (8), electrons in the valence band differ from those in the conduction band only in different relations between the amplitudes of the Bloch waves from which their wave functions are formed. Assuming that the valence band is filled to infinitely large momenta, some perturbation-theory diagrams of the electron–electron interaction diverge. In reality, the valence band is filled to momenta p_c, of the order of the reciprocal lattice vector, which are greater by several orders of magnitude than any other momenta encountered in problems involving electron properties. As a result of this factor, some diagrams make finite but still very large contributions to the perturbation theory series.

For instance, the simplest exchange diagram for the electron self-energy gives [59]

$$\Sigma(p) = \frac{e^2}{\varepsilon}\, p \ln \frac{p_c}{p}\,, \tag{10}$$

where ε is the dielectric permittivity of the medium surrounding graphene (if graphene is sandwiched between two different media with permittivities ε_1 and ε_2, then ε is replaced with $(\varepsilon_1 + \varepsilon_2)/2$). This results in an unusual logarithmic renormalization of the Fermi velocity in the range of small momenta. It was shown that this result persists in higher orders of the perturbation theory [60].

As follows from the linear dispersion of electrons in graphene, the density of states behaves as $\mathcal{N} \propto |E|$ and vanishes at the Dirac point $E = 0$ (in contrast to $\mathcal{N} = \text{const}$ in a quasi-two-dimensional system with a parabolic dispersion law). The chemical potential in undoped graphene is at the Dirac point. Then, any external perturbation not only affects charge carriers but also creates these carriers by polarizing the filled valence band. Consequently, the response of undoped graphene to external perturbations must be of a nonlinear type. For example, the static screening calculated for undoped graphene in the linear-response approximation is of the semiconductor type [61]. But going beyond the linear approximation shows that in reality the screening is strong and essentially nonlinear [28, 62].

The zero gap between the valence band and the conduction band points to the possibility of restructuring the ground state of the electron system as a result of the spontaneous formation of a condensate of electron–hole pairs, resembling the state of an excitonic insulator [63]. Papers [64] considered how the possibility of this instability of the ground state of graphene depends on the parameter N, the number of spin components of electrons. It was shown that although a phase transition does not occur at the realistic value $N = 2$, the closeness to this value may lead to appreciable fluctuations in the corresponding order parameter.

Another feature of multiparticle effects in graphene stems from the linear dispersion because it causes the kinetic energy of the electron gas in graphene per particle to be $\hbar v_F/l$ by an order of magnitude, where l is the mean distance between particles. The potential energy of the Coulomb interaction is $e^2/(\varepsilon l)$ by the order of magnitude. The dimensionless parameter r_s determining the ratio of the typical values of the Coulomb and kinetic energies of a quantum system takes the following form in the case of graphene:

$$r_s = \frac{e^2}{\varepsilon \hbar v_F} \approx \frac{2.19}{\varepsilon}\,.$$

As we see, this parameter is independent of the concentration of the electron gas! The only way of affecting it is to somehow change the ambient dielectric permittivity ε. The parameter r_s can vary in a fairly limited range (e.g., if graphene is on a substrate of SiO_2 with $\varepsilon \approx 4.5$ and is surrounded by air on the other side, then $r_s \approx 1$, and if graphene is immersed in HfO_2 with $\varepsilon \approx 25$, then $r_s \approx 0.1$).

We note for comparison that the mean kinetic energy in a two-dimensional or three-dimensional electron gas with the quadratic dispersion is proportional to l^{-2}. Consequently, $r_s \propto l$ and decreases with increasing the density, and the Coulomb interaction energy in a sufficiently dense gas can be regarded as a small correction to the kinetic energy. If we consider only realistic values of r_s, the applicability of the perturbation theory conditions to graphene is still doubtful. Moreover, it is impossible to achieve very high values of r_s in graphene, and therefore impossible to create strongly correlated states, including the Wigner crystallization, without a magnetic field [65] (however, a magnetic field can induce Wigner crystallization in graphene [66] and in a quasi-two-dimensional electron gas [67]).

The possibility of varying r_s by placing graphene into media with different values of the dielectric permittivity ε suggests that this method may allow controlling its collective electron properties. Furthermore, the electron–electron interaction in graphene, whose strength is inversely proportional to ε, renormalizes the Fermi velocity [68] (by some estimates [69], it amounts to 15–20% of the bare value). As a result, the Fermi velocity must be rather sensitive to the properties of the ambient medium, and this may be used for creating contactless sensors.

Collective effects in graphene placed in a magnetic field are also rather special. The magnetic field of a strength H determines the 'magnetic length' $l_H = (\hbar c/eH)^{1/2}$, a parameter with the dimension of length, corresponding to the radius of cyclotron orbits of electrons. The characteristic Coulomb energy per particle is of the order of $e^2/\varepsilon l_H$. In a quasi-two-dimensional electron gas, the distance between Landau levels that corresponds to the characteristic kinetic energy is $\hbar eH/(mc)$. Therefore, the kinetic energy dominates in sufficiently strong magnetic fields and the Coulomb interaction energy is a weak perturbation. Hence, the mixing of different Landau levels in a quasi-two-dimensional electron gas in strong magnetic fields is negligible and each level can be considered isolated [70, 71]. The effective mass of the electron in graphene is zero and therefore the distance between Landau levels is determined by the magnetic length; it is of the order of $\hbar v_F/l_H$. As can be readily shown, the ratio of the potential energy to the kinetic energy is independent of the field strength H and can be regulated only by the dielectric permittivity ε of the ambient medium. Therefore, in dealing with graphene, the concept of 'strong magnetic fields' must be used with care.

5. Bardeen–Cooper–Schrieffer pairing in an electron–hole bilayer

In this section, we consider superfluidity related to the electron–hole pairing in a graphene bilayer (see [72]). In this context, we define a bilayer not as two-layer graphene but as two parallel graphene sheets separated by an insulating layer of thickness D (D is sufficiently large to allow ignoring tunneling between the sheets). The prescribed concentration of charge carriers and the corresponding chemical potential μ in each of the layers can be established by using two independent electrodes (Fig. 4). We here consider the case of

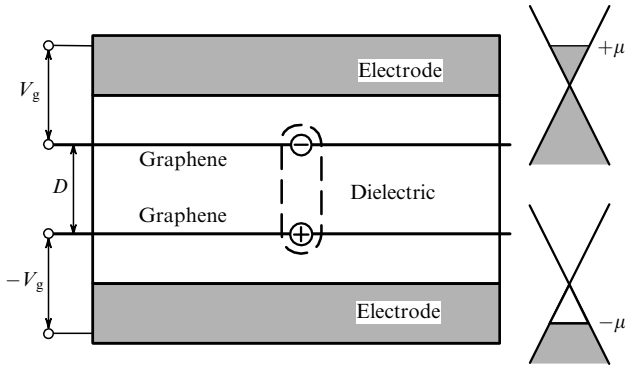

Figure 4. Schematic diagram of a system for implementing the pairing of spatially separated electrons and holes in a graphene bilayer. The right-hand side of the figure shows the positions of the chemical potential in two layers of graphene controlled by two gate voltages V_g and $-V_g$.

equal carrier densities when the chemical potential in the upper layer has a value $\mu > 0$ and charge carriers are electrons, while in the lower layer, the chemical potential is $-\mu < 0$ and the charge carriers are holes.

This electron–hole system is shown to be unstable with respect to the interlayer pairing of electrons and holes owing to their Coulomb attraction. Closely analogous to this pairing are the pairing of electrons with opposite spins in conventional superconductors as described by the Bardeen–Cooper–Schrieffer (BCS) theory [73], and the electron–hole pairing in excitonic insulator [63], where there is in fact no superfluidity of pairs because the phase of the order parameter is fixed (it is related to interband transitions). The problem of electron–hole pairing in a system of two coupled quantum wells that contain a quasi-two-dimensional electron gas with a quadratic dispersion was analyzed theoretically in [74, 75].

We consider the effective Hamiltonian of the system responsible for the pairing of electrons in the upper graphene layer with holes in the lower layer. The effect of the part of the Hamiltonian that corresponds to the interaction between electrons and holes within individual layers manifests itself through interlayer screening of the electron–hole interaction. The effective Hamiltonian corresponding to the pairing of quasiparticles with opposite momenta has the form

$$H = g_s g_v \sum_{\mathbf{p}} \xi_{\mathbf{p}} (a_{\mathbf{p}}^+ a_{\mathbf{p}} + b_{\mathbf{p}}^+ b_{\mathbf{p}}) + \frac{g_s g_v}{S} \times \sum_{\mathbf{p},\mathbf{q}} V(\mathbf{q}) \frac{1+\cos\varphi}{2} a_{\mathbf{p}+\mathbf{q}}^+ b_{-\mathbf{p}-\mathbf{q}}^+ b_{-\mathbf{p}} a_{\mathbf{p}} , \quad (11)$$

where $a_{\mathbf{p}}$ and $b_{\mathbf{p}}$ are annihilation operators for Dirac electrons and holes with momentum $\mathbf{p}$, $\xi_{\mathbf{p}} = v_F|\mathbf{p}| - \mu$ is the energy of particles relative to the Fermi level, $V(\mathbf{q})$ is the potential of the screened electron–hole interaction, $\mathbf{q}$ is the momentum transferred in an act of scattering, φ is the angle between $\mathbf{p}$ and $\mathbf{p}+\mathbf{q}$, that is, the scattering angle of the electron and hole, and S is the area of the system. The angle factor $(1+\cos\varphi)/2$, specific for graphene, appears as a result of folding of the electron and hole wave functions of form (8) over spinor components in the states before and after the scattering event (see Section 3). The coefficients $g_s = g_v = 2$ represent degeneracy of electron states in spin and valleys.

Diagonalization of Hamiltonian (11) using a Bogolyubov transformations gives a self-consistent equation for the gap,

$$\Delta_{\mathbf{p}} = -\frac{1}{4\pi^2} \int d\mathbf{q} V(\mathbf{q}) \frac{1+\cos\varphi}{2} \frac{\Delta_{\mathbf{p}+\mathbf{q}}}{2E_{\mathbf{p}+\mathbf{q}}} , \quad (12)$$

where $E_{\mathbf{p}} = (\xi_{\mathbf{p}}^2 + \Delta_{\mathbf{p}}^2)^{1/2}$. We note that two specific features distinguish Eqn (12) from its analog in coupled quantum wells. The first is the linear dependence of $\xi_{\mathbf{p}}$ on $\mathbf{p}$ instead of the quadratic one in coupled quantum wells. The second feature is the presence of the angle factor $(1+\cos\varphi)/2$ that suppresses backscattering in graphene. In the case of weak coupling, this coefficient differs only slightly from unity because small scattering angles dominate in the integral in Eqn (12); however, it may weaken the pairing in the case of strong coupling.

The main contribution to the integral in Eqn (12) is obtained in the vicinity of the Fermi energy in which the dynamically screened interlayer electron–hole interaction $V(\mathbf{q},\omega)$ is attractive. In the linear-response approximation, we have

$$V(\mathbf{q},\omega) = \frac{-v_{\mathbf{q}} \exp(-qD)}{1 - v_{\mathbf{q}}(\Pi_1 + \Pi_2) + v_{\mathbf{q}}^2 \Pi_1 \Pi_2 [1 - \exp(-2qD)]} , \quad (13)$$

where Π_1 and Π_2 are dynamic polarization operators of the upper and lower layers of graphene. In the case of equal densities, polarizability of both layers of graphene is identical owing to the symmetry between electrons and holes: $\Pi_1 = \Pi_2 = \Pi$. The equation obtained by setting the denominator in (13) equal to zero describes two branches $\omega_\pm(q)$ of plasmon dispersion in the bilayer; the branches correspond to plasma oscillations that are in-phase and anti-phase in the two layers of graphene [61, 74, 76].

The weak-coupling (or BCS) regime is realized if the width of the pairing region near the Fermi energy is small in comparison with the Fermi energy. In this case, we can decouple the radial integration in the variable $\xi \equiv \xi_{\mathbf{p}+\mathbf{q}}$ in Eqn (12) for the gap and the integration over the polar angle φ. In the spirit of the BCS theory, we integrate over ξ in the region restricted by the cutoff energy $\hbar\tilde{\omega}$, where dynamically screened interaction (13) is attractive. We now assume that the main contribution to the integral in φ comes from small q that do not exceed the values of $\tilde{q}$ at which the static interaction $V(\mathbf{q}) \equiv V(\mathbf{q},0)$ decreases by a factor of two, $V(\tilde{q}) = V(0)/2$, by more than an order of magnitude. The explicit form of $V(\mathbf{q})$ is determined by the static polarizability [61, 62, 77]

$$\Pi(\mathbf{q},0) = -\frac{g_s g_v \mu}{2\pi\hbar^2 v_F^2} \equiv -\frac{\varepsilon}{\pi e^2 a} , \quad (14)$$

where a is the Thomas–Fermi screening length in graphene.

We introduce the Fermi momentum $k_0 = \mu/\hbar v_F$ and the dimensionless parameter

$$\alpha = \frac{2\varepsilon\hbar v_F}{g_s g_v e^2} = \frac{1}{2r_s} \approx 0.23\,\varepsilon .$$

The system under consideration has three characteristic lengths: a, D, and the mean distance $l \sim 1/k_0$ between charge carriers in each of the graphene layers. The behavior of the system depends on the relative values of a, D, and l. It can be shown that $a/l = \alpha$ and $D/l = k_0 D$. Hence, the behavior of the system is determined by two dimensionless parameters, α and $k_0 D$.

It follows from (13) and (14) that the value of the characteristic momentum $\tilde{q}$ is determined either by the cutoff owing to the presence of the factor $\exp(-qD)$ in the numerator of (13) or by the Thomas–Fermi screening in the denominator:

$$\tilde{q} = \min\left(\frac{4k_0}{\alpha}, \frac{2}{D}\right). \tag{15}$$

The cutoff energy $\hbar\tilde{\omega}$ is determined by the characteristic frequency of the lower branch of plasma oscillations and can be estimated as $\hbar\tilde{\omega} = \hbar\omega_-(\tilde{q})$. In the first order in the electron–electron interaction, the dynamic polarizability for $q \to 0$ and $\omega > v_F q$ is [61, 77]

$$\Pi(\mathbf{q}, \omega) = \frac{g_s g_v \mu q^2}{4\pi\hbar^2\omega^2}. \tag{16}$$

For $\alpha \ll k_0 D$, we have $\omega_-(q) = v_F q\,(k_0 D/\alpha)^{1/2}$ and $\omega_+(q) = v_F(2k_0 q/\alpha)^{1/2}$. Hence, the cutoff energy equals $\hbar\tilde{\omega} = 2\mu/(k_0 D\alpha)^{1/2}$. In the case $\alpha \gg k_0 D$, approximate expression (16) cannot be used because the lower branch of plasma oscillations found from (16) falls into the range of one-particle excitations $\omega < v_F q$. Indeed, in this case, $\omega_-(q) = v_F q$ and $\omega_+(q) = v_F(2k_0 q/\alpha)^{1/2}$, and the cutoff energy equals $\hbar\tilde{\omega} = 4\mu/\alpha$.

The size of the electron–hole Cooper pairs is of the order of $1/\tilde{q}$ in the direction parallel to the graphene layers. The weak-coupling regime requires the mean distance between neighbor pairs to be small in comparison with the size of a single pair, that is, $\tilde{q}l \ll 1$. Using (15), we can conclude that the weak-coupling regime occurs when at least one of the parameters α or $k_0 D$ is much greater than unity.

In our case, pairing need not necessarily be s-wave. Because of the spatial separation of electrons and holes, the Pauli principle does not impose any constraints on either the mutual orbital momentum or the spins and valleys of pairing particles. We seek the l-wave solution of (12) assuming that $\Delta_{\mathbf{p}} = \Delta\exp(\mathrm{i}l\varphi_{\mathbf{p}})$ for $|\xi| \leqslant \hbar\tilde{\omega}$ and $\Delta_{\mathbf{p}} = 0$ for $|\xi| > \hbar\tilde{\omega}$. The approximate solution has the form

$$\Delta = 2\hbar\tilde{\omega}\,\exp\left\{-\frac{4\pi\alpha}{V_l}\right\}. \tag{17}$$

The dimensionless l-wave harmonic of the potential $V(\mathbf{q})$ with the angle factor incorporated takes the form

$$V_l = \int_0^{2\pi} \frac{\exp(-k_0 Dx)(1+\cos\varphi)/2}{x + 4/\alpha + 4\left[1-\exp(-2k_0 Dx)\right]/\alpha^2 x} \times \exp(-\mathrm{i}l\varphi)\,\mathrm{d}\varphi, \tag{18}$$

where $x = q/k_0 = 2\sin(\varphi/2)$.

Condensation occurs at a value of l at which the harmonic V_l is the largest. We found numerically that the s-wave pairing dominates for all values of α and $k_0 D$ even though the difference between the values of V_l and the neighboring values of l becomes very small if the coupling is very weak. In what follows, we consider only the s-wave pairing. We calculate the gap width for different ratios of α, $k_0 D$, and unity by deriving asymptotic expressions for V_l and substituting them in (17).

If $\alpha \ll k_0 D$, then

$$\Delta = \frac{4\mu}{(k_0 D\alpha)^{1/2}}\exp\left[-8\pi k_0 D\left(1+\frac{k_0 D}{\alpha}\right)\right]. \tag{19}$$

Expression (19) is applicable for values of α both greater than unity and much smaller than unity.

If $\alpha \gg k_0 D$, we distinguish between the cases of small and intermediate interlayer distances. In the former case, in which $k_0 D \ll 1 \ll \alpha$, the gap is

$$\Delta = \frac{8\mu}{\alpha}\exp\left\{-\frac{2\pi\alpha}{\ln(1+\alpha/2)}\right\}. \tag{20}$$

In the latter case, that is, when $1 \ll k_0 D \ll \alpha$, we have

$$\Delta = \frac{8\mu}{\alpha}\exp\left\{-\frac{\pi\alpha/2}{\ln(\alpha/4k_0 D) - \gamma}\right\}, \tag{21}$$

where $\gamma \approx 0.577$ is the Euler constant.

We have considered the case of weak coupling; what if the coupling is strong? In systems of pairing fermions (e.g., in a cooled system of Fermi atoms), the crossover from the BCS-like state to Bose–Einstein condensation (BEC) in a rarefied gas of localized nonoverlapping pairs occurs as the coupling strength increases [78]. Likewise, in the case of strong coupling in coupled quantum wells with electrons and holes at $T = 0$, crossover occurs to the BEC of the rarefied gas of localized electron–hole pairs (or excitons in a quasiequilibrium state created by laser pumping). If $T \neq 0$, both the BCS-like state and the gas of local pairs are in a superfluid state at temperatures below the Kosterlitz–Thouless transition to the normal state [6, 75]. A graphene bilayer cannot have localized electron–hole pairs because there is no gap in the energy spectrum. Hence, the behavior of the graphene electron–hole bilayer is radically different from the behavior characterized by the BCS–BEC crossover in coupled quantum wells. It can be expected that what we then obtain would be a kind of 'ultrarelativistic' BCS state with a fairly high critical temperature.

In recent paper [79], an equation for the gap was considered taking the cone-shaped band structure of graphene into account but not including the angle factor, in contrast to (12). The integration in the equation covered both energy bands, which corresponds to the case of strong coupling. We considered the case of weak coupling in which only the conduction band of the upper graphene layer and the valence band of the lower layer are involved, and hence the contribution of interband transitions is not accounted for in the equation for the gap width. However, all four bands must be taken into account in the case of strong coupling, and therefore the gap equation must have a matrix form with respect to band indices (this was not done in [79]).

We consider the conditions of weak coupling for $\alpha \ll 1$ and $\alpha \sim 1$ more carefully. Such values of α can be realized, for example, with the traditionally used substrate of SiO_2 ($\varepsilon \approx 4.5$). The coupling strength is then determined only by the value of $k_0 D$. The Fermi momentum k_0 is proportional to the chemical potential μ, which in an electrically doped graphene can be varied from zero to the maximum value ≈ 0.3 eV [10]. The weak-coupling regime ($k_0 D \gg 1$) can be achieved at reasonable concentrations of charge carriers at interlayer spacings $D > 100$ Å. On the other hand, the strong-coupling regime can always be realized by letting μ tend to zero. Therefore, the transition from weak to strong coupling can always be traced experimentally by varying the gate voltage.

The case of $\alpha \gg 1$ is realized at large values ($\varepsilon > 5$) of the dielectric permittivity ε of the ambient medium and can be observed, for instance, using HfO_2 ($\varepsilon \approx 25$). In this case, the

weak-coupling regime survives even as $\mu \to 0$, i.e., at arbitrarily low concentrations of charge carriers; according to formula (20), the gap then tends to zero as $\Delta \propto \mu$. This situation differs greatly from that in coupled quantum wells, where the strong-coupling regime sets in inevitably at vanishingly low charge concentrations.

With a typical value of the chemical potential $\mu \approx 0.1$ eV and a relatively small interlayer separation $D = 50$ Å and with $\varepsilon = 7$ (the weak-coupling approximation is still sufficiently reliable), we find the gap width $\Delta = 4 \times 10^{-6}$ eV, which is equivalent to the temperature 0.05 K. The maximum gap width can be obtained in the strong-coupling regime when $\alpha \sim k_0 D \sim 1$. Then the gap may reach $\Delta \sim \mu$, up to several hundred kelvins.

The electron–hole pairing in a graphene bilayer in the Hartree–Fock approximation was recently considered in [80]. Calculations of the Kosterlitz–Thouless transition temperature also showed that it may reach room temperature. But the situation treated in [80] is definitely the strong-coupling case and requires both taking dynamic effects into account and considering the bands not involved in the case of weak coupling. Nevertheless, the arguments offered above permit us to hope that in the strong-coupling situation, the superconducting transition temperature may indeed reach high values.

We now evaluate the effect of impurities and disorder. In the case of traditional phonon-mediated superconductivity, the presence of magnetic impurities acts destructively on the BCS state, because they differently influence the electrons with antiparallel spins forming a Cooper pair. In our case, any impurity in any layer of graphene acts destructively on the condensate of pairs because it scatters only one component of the pair. Our calculations show that the critical transition temperature T_c found using the Matsubara diagram technique (and yielding an upper bound on the Kosterlitz–Thouless transition temperature) is given by

$$T_c = T_c^{(0)} - \frac{\hbar}{2\pi\tau},$$

where $T_c^{(0)} = \Delta_{T=0}/2\pi$ is the transition temperature in the absence of impurities and τ is the mean free time [81]. Therefore, the BCS-like state is destroyed when $\tau > \hbar/\Delta$. The expression for diffusional conductivity [82] yields $\tau \approx (\mu/ev_F^2)\mu_c$, where μ_c is the mobility of charge carriers in graphene. Conductivity in 'dirty' graphene specimens was $\mu_c \approx 1000$ cm^2 B^{-1} s at room temperature [8] and the mean free time $\tau \approx 10^{-14}$ s corresponds to the gap $\Delta \approx 0.07$ eV. Contrarily to this, in pure graphene at liquid helium temperature, $\mu_c \approx 10^6$ cm^2 B^{-1} s, and hence $\tau \approx 10^{-11}$ s corresponds to the gap $\Delta \approx 7 \times 10^{-5}$ eV. Comparing this last value with the above estimates of gap width in different regimes, we find that the BCS-like state in the weak-coupling regime can be implemented only in sufficiently pure specimens of graphene. At the same time, in the case of strong coupling, the condensate can survive despite a fairly strong disorder.

The creation of a superfluid phase with electron–hole pairing can be revealed experimentally by the emergence of special features in the effect of Coulomb drag caused by changing the temperature. It was shown for coupled quantum wells that the condensation of pairs results in an increase in the drag coefficient [83, 84]. Another method of detecting the condensate consists in observing effects similar to the Josephson effect (see [85] and the references therein). Furthermore, condensation changes the nature of the system response to an external electromagnetic field. Thus, an external magnetic field applied parallel to the graphene layer plane results in the generation of nondecaying currents, which can be detected in a straightforward manner [74, 85, 86].

6. Bose condensation and superfluidity of magnetoexcitons in graphene

We now consider an electron–hole bilayer, the same as in Section 5 but placed in a magnetic field perpendicular to it. As we mentioned in Section 5, localized electron–hole pairs cannot form in a graphene bilayer because there is no gap in the band spectrum. In a magnetic field, electrons group at the Landau levels [38] and a gap emerges in the spectrum such that localized magnetoexcitons can form [87]. In this section, we consider Bose condensation and superfluidity of the gas of magnetoexcitons in the graphene bilayer (see [88]).

A certain concentration of magnetoexcitons in a bilayer can be created both by an equilibrium method regulating the degree of filling the Landau levels by the electric field of control electrodes, and in a quasiequilibrium manner using laser pumping. Because of a relatively large distance between the layers, the recombination of charge carriers is greatly suppressed and we can speak of quasiequilibrium chemical potentials of electrons and holes.

The role of the net momentum of an electron–hole pair in a magnetic field is played by the conserved magnetic momentum [89] $\mathbf{P} = \mathbf{p}_e + \mathbf{p}_h + (e/c)(\mathbf{A}_e - \mathbf{A}_h) - (e/c)[\mathbf{H} \times (\mathbf{r}_e - \mathbf{r}_h)]$. The conservation of $\mathbf{P}$ is caused by the invariance of the Hamiltonian of the system under two-dimensional translations combined with simultaneous gauge transformation [90]. A magnetoexciton state is specified by the indices n_1 and n_1 of the Landau levels of the electron and hole forming it, as well as by its magnetic momentum $\mathbf{P}$. The operator of Coulomb interaction between spatially separated electron and hole has the form $V(r) = -e^2/\varepsilon(\mathbf{r}^2 + D^2)^{1/2}$, where $\mathbf{r} = \mathbf{r}_e - \mathbf{r}_h$ is the two-dimensional radius vector parallel to the graphene layers. We now assume that the Coulomb interaction energy is small in comparison with the distance between Landau levels (we later establish the applicability conditions of this approximation); in this case, the energy of a magnetoexciton can be calculated in the first order of the perturbation theory [87]:

$$\begin{aligned} E_{n_1,n_2} = 2^{\delta_{n_1,0}+\delta_{n_2,0}-2}\Big[& E^{\mathrm{CQW}}_{|n_1|,|n_2|} + (1-\delta_{n_1,0})\, E^{\mathrm{CQW}}_{|n_1|-1,|n_2|} \\ & + (1-\delta_{n_2,0})\, E^{\mathrm{CQW}}_{|n_1|,|n_2|-1} \\ & + (1-\delta_{n_1,0})(1-\delta_{n_2,0})\, E^{\mathrm{CQW}}_{|n_1|-1,|n_2|-1}\Big]. \end{aligned} \tag{22}$$

Here, $E^{\mathrm{CQW}}_{|n_1|,|n_2|}$ is the energy of such a magnetoexciton in coupled quantum wells [70, 91] whose electron is at the $|n_1|$th Landau level and the hole is at the $|n_2|$th level. In the approximation of a weak Coulomb interaction, this energy equals the mean value of the operator $V(r)$ in the eigenstate of the nonrelativistic Hamiltonian of the electron–hole pair. For low magnetic momentum satisfying the conditions $P \ll \hbar/l_H$ and $P \ll \hbar D/l_H^2$, we obtain [91]

$$E^{\mathrm{CQW}}_{|n_1|,|n_2|} \approx \mathcal{E}^{\mathrm{CQW}}_{|n_1|,|n_2|} + \frac{P^2}{2M^{\mathrm{CQW}}_{|n_1|,|n_2|}},$$

where the binding energy of a 'nonrelativistic' magnetoexciton $\mathcal{E}^{\mathrm{CQW}}_{|n_1|,|n_2|}$ and its effective magnetic mass $M^{\mathrm{CQW}}_{|n_1|,|n_2|}$ are

functions of the parameters H and D of the system. Substituting this expansion in (22), we can find the effective mass M_{n_1,n_2} and the binding energy $\mathcal{E}_{n_1,n_2}$ of the magnetoexciton in a graphene bilayer as functions of H and D.

The mean-square radius of a magnetoexciton at rest at moderately large quantum numbers n_1 and n_2 is of the order of several magnetic lengths. At large distances between layers, $D \gg l_H$, the binding energy $\mathcal{E}^{\mathrm{CQW}}_{|n_1|,|n_2|}$ and the effective mass $M^{\mathrm{CQW}}_{|n_1|,|n_2|}$ of nonrelativistic magnetoexcitons at arbitrary $|n_1|$ and $|n_2|$ reach universal asymptotic levels $\mathcal{E}^{\mathrm{CQW}} = -e^2/(\varepsilon D)$ and $M^{\mathrm{CQW}} = \varepsilon D^3 H^2/c^2 = \varepsilon D^3 \hbar^2/(e^2 l_H^4)$. Therefore, according to (22), the binding energy and the effective mass of the magnetoexciton in a graphene bilayer reach the same asymptotic levels:

$$\mathcal{E} = -\frac{e^2}{\varepsilon D}, \qquad M = \frac{\varepsilon D^3 \hbar^2}{e^2 l_H^4}\,. \tag{23}$$

Hence, at low P, the magnetoexciton energy referenced to its binding energy is given by $\epsilon(P) = P^2/(2M)$. If D is greater than the mean distance $\langle r\rangle$ between the electron and the hole in the bilayer plane, the magnetoexcitons can be regarded as interacting electric dipoles aligned in parallel. In a magnetic field, there is a link between the motion of the center of mass of the magnetoexciton and its internal structure [70], resulting in the expression $\langle r\rangle = P l_H^2/\hbar$ (in other words, the electric field $\mathbf{E} = [\mathbf{v}\times\mathbf{H}]/c$ emerges in the reference frame of the exciton moving in the magnetic field at a velocity $\mathbf{v}$ and polarized by this field). If the concentration of magnetoexcitons with the parabolic dispersion is n, the typical values of magnetic momenta are $P \sim \hbar\sqrt{n}$. Therefore, the relation $D \gg \langle r\rangle$ holds for $D \gg l_H^2\sqrt{n}$. In this situation, one of the conditions of applicability of the effective-mass approximation holds: $P \ll \hbar D/l_H^2$. The second condition $P \ll \hbar/l_H$ holds if $l_H\sqrt{n} \ll 1$. We immediately see that the mean square radius of the magnetoexciton at rest, equal by an order of magnitude to l_H, is much smaller than the mean distance $n^{-1/2}$ between particles. Finally, we recall the above condition of smallness of the Coulomb interaction in comparison with the separation between Landau levels. This condition implies that $e^2/\varepsilon D \ll \hbar v_{\mathrm{F}}/l_H$ or $D \gg r_{\mathrm{s}} l_H$.

We pointed out in Section 4 that the degree of mixing of Landau levels in graphene is independent of the magnetic field strength because the characteristic values of both the Coulomb energy and the kinetic energy are proportional to $H^{1/2}$. But the characteristic value of the kinetic energy in a graphene bilayer remains proportional to $H^{1/2}$, while the characteristic energy of the interlayer Coulomb interaction ceases to depend on H for $D \gg l_H$ and is determined by the distance D.

We therefore derived that if $D \gg l_H$ and $l_H\sqrt{n} \ll 1$ (i.e., for a sufficiently low concentration, large separation between layers, and a strong magnetic field) magnetoexcitons behave as dipoles aligned in parallel and have the effective mass M. Magnetoexcitons interact with one another via the repulsive dipole – dipole potential [75, 92] $U(R) = e^2 D^2/(\varepsilon R^3)$. Both the overlapping of the wave functions of neighboring excitons and the mixing of Landau levels are negligibly small, and this allows projecting the state of the system onto the lower Landau levels of electrons and holes. As a result, the matrix Hamiltonian of the electron – hole pair (over the electron and the hole sublattices) reduces to its scalar projection onto the lower Landau levels. Consequently, under the conditions listed above, magnetoexcitons form a weakly nonideal Bose gas of repulsive dipoles.

At $T = 0$, the weakly nonideal Bose gas of magnetoexcitons forms a Bose condensate [93]. An adequate approximation for the rarefied system is the summation of ladder diagrams for the interexciton dipole – dipole interaction. By analogy to [74, 94] (see also [95]), we can write the equation for the vertex part with the magnetic mass playing the role of mass and the magnetic momentum playing the role of momentum:

$$\Gamma(\mathbf{p},\mathbf{p}';\mathbf{P},\Omega) = \tilde{U}(\mathbf{p}-\mathbf{p}') + \int \frac{\mathrm{d}\mathbf{q}}{(2\pi\hbar)^2}\,\frac{\tilde{U}(\mathbf{p}-\mathbf{q})\,\Gamma(\mathbf{q},\mathbf{p}';\mathbf{P},\Omega)}{(\varkappa^2/M)+\Omega-\mathbf{P}^2/(4M)-q^2/M+\mathrm{i}\delta}\,,$$

$$\mu = \frac{n}{4}\,\Gamma(0,0;0,0)\,, \tag{24}$$

where $\mu \equiv \varkappa^2/2M$ is the chemical potential of the system, $\tilde{U}(\mathbf{p})$ is the Fourier transform of the interaction potential $U(R)$, and $\delta \to 0^+$. A simple analytic solution of Eqn (24) can be obtained for the chemical potential such that $U(\varkappa) \ll \mu$. In accordance with the asymptotic expression for the magnetic mass, this condition is satisfied if $(D/l_H)^5 \ll 1/(l_H\sqrt{n})$. Then,

$$\mu = \frac{\pi\hbar^2 n}{M\ln\left[\hbar^4\varepsilon^2/(2\pi n M^2 e^4 D^4)\right]}\,. \tag{25}$$

For small magnetic momenta, Eqn (24) yields the acoustic spectrum of collective excitations $\epsilon(P) = c_{\mathrm{s}}P$, where $c_{\mathrm{s}} = \sqrt{\mu/M}$ is the speed of sound and μ is given by (25). The acoustic spectrum arises due to the dipole – dipole repulsion of magnetoexcitons and satisfies the Landau superfluidity criterion, which allows the magnetoexciton superfluidity in a graphene bilayer at low temperatures. A transition of the two-dimensional weakly nonideal Bose gas from the normal to the superfluid state is a Kosterlitz – Thouless transition [6]. The temperature T_{KT} of this transition is found from the expression $T_{\mathrm{KT}} = \pi\hbar^2 n_{\mathrm{s}}(T_{\mathrm{KT}})/(2k_{\mathrm{B}}M)$, where n_{s} is the density of the superfluid component as a function of temperature and k_{B} is the Boltzmann constant.

The superfluid density can be found as $n_{\mathrm{s}} = n/4 - n_{\mathrm{n}}$, where n_{n} is the density of the normal component and the total density n is divided by 4 to take the additional degeneracy in valleys into account (additional in comparison with the degeneracy in coupled quantum wells). The value of n_{n} can be found using the Landau procedure (see, e.g., [93, 96]) as a linear response of the total current in the system to the external velocity field (in this approximation, the normal component is dominated by the gas of noninteracting excitations):

$$n_{\mathrm{n}}(T) = \frac{3\zeta(3)}{2\pi\hbar^2}\,\frac{k_{\mathrm{B}}^3 T^3}{M c_{\mathrm{s}}^4}\,, \tag{26}$$

where $\zeta(z)$ is the Riemann zeta function ($\zeta(3) \approx 1.202$). Ultimately, we arrive at the following expression for the transition temperature:

$$T_{\mathrm{KT}} = \frac{T_{\mathrm{KT}}^0}{2^{1/3}}\left\{\left[1+\sqrt{\frac{32}{27}\left(\frac{4Mk_{\mathrm{B}}T_{\mathrm{KT}}^0}{\pi\hbar^2 n}\right)^3+1}\right]^{1/3} - \left[\sqrt{\frac{32}{27}\left(\frac{4Mk_{\mathrm{B}}T_{\mathrm{KT}}^0}{\pi\hbar^2 n}\right)^3+1}-1\right]^{1/3}\right\}. \tag{27}$$

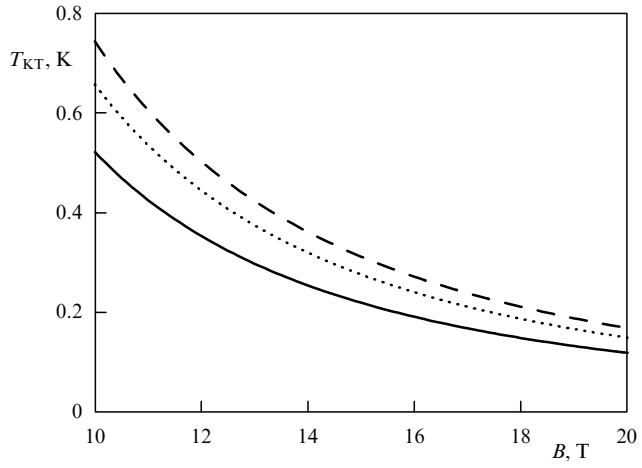

Figure 5. The Kosterlitz–Thouless transition temperature T_{KT} as a function of the magnetic field B in a graphene bilayer separated by SiO_2 ($\varepsilon \approx 4.5$). The concentration of magnetoexcitons is $n = 4 \times 10^{11}$ cm^{-2}. The separation D between layers is 30 nm (solid curve), 28 nm (dotted curve), and 27 nm (dashed curve).

Here, $T^0_{KT} = k_B^{-1}[\pi\hbar^2 n c_s^4 M/6\zeta(3)]^{1/3}$ is an auxiliary quantity equal to the temperature at which the superfluid density vanishes in the mean-field approximation, i.e., $n_s(T^0_{KT}) = 0$.

The temperature T^0_{KT} as a function of the parameters H and D of the system can be used to evaluate the crossover region in which local superfluid density manifests itself for magnetoexcitons on scales smaller than or of the order of the mean distance between vortices in the system. The local superfluid density can manifest itself in local optical or transport properties. As a function of the magnetic field and density, T_{KT} is plotted in Fig. 5. According to (27), the temperature of the transition to a superfluid state *at a fixed density of magnetoexcitons* decreases as the magnetic field strength H and the interlayer distance D increase, which is explained by the magnetic mass M increasing as a result of increasing H and D. For $D \gg l_H$, the value of T_{KT} decreases as H^{-2}.

The effective magnetoexciton mass in a graphene bilayer, not constrained by the masses of its constituent electron and hole, can be made very small. Because the temperature of the transition to a superfluid state is inversely proportional to the mass, studying the BEC of magnetoexcitons in graphene bilayers may prove to be simpler than in coupled quantum wells.

7. Collective properties of magnetoexcitons in a three-layer system

In this section, we discuss the main results in papers [97, 98] treating BEC and the superfluidity of magnetoexcitons in a three-layer system.

We consider a system forming a stack of three graphene layers separated by insulating layers, which prevent rapid recombination of electrons and holes from different graphene layers. We assume that layers with electrons and holes alternate (this can be achieved by either electric doping with gate electrodes or the chemical doping of graphene layers). In this case, the dipole moments of magnetoexcitons formed by charges of one pair of layers are aligned in parallel, and the dipole moments of magnetoexcitons from the neighboring pairs of layers are aligned in antiparallel fashion. This situation, typical of a three-layer system of the e–h–e or h–e–h type, differs from the case of the electron–hole bilayer, in which the magnetoexciton system is stable owing to the dipole–dipole repulsion.

We consider the BEC and superfluidity of magnetobiexcitons (i.e., of coupled states of pairs of magnetoexcitons with oppositely oriented dipole moments). The interaction of magnetobiexcitons at large distances, as the interaction of electric quadrupoles, is repulsive and ensures the stability of their system.

We work in the approximations described in Section 6: for $D \gg l_H$ and $l_H\sqrt{n} \ll 1$, magnetoexcitons behave as bosons of a mass M, whose role is played by the effective magnetic mass. In the low-density limit, two magnetoexcitons aligned in the parallel or antiparallel manner at a distance R interact via the respective potentials $U_+(R)$ or $U_-(R)$.

The effective Hamiltonian of the system of magnetoexcitons in the above approximation can be written as $H_{tot} = H_0 + H_{int}$. The effective Hamiltonian H_0 of the system of noninteracting magnetoexcitons has the form

$$H_0 = \frac{1}{2}\sum_{\mathbf{p}} \epsilon_0(p)\left(a^+_{\mathbf{p}} a_{\mathbf{p}} + b^+_{\mathbf{p}} b_{\mathbf{p}} + a^+_{-\mathbf{p}} a_{-\mathbf{p}} + b^+_{-\mathbf{p}} b_{-\mathbf{p}}\right),$$

where $\epsilon_0(p) = p^2/2M$ is the energy of noninteracting magnetoexcitons, $\mathbf{p}$ is the magnetic momentum, and $a_{\mathbf{p}}$ and $b_{\mathbf{p}}$ are operators of annihilation of magnetoexcitons with dipole moments respectively oriented upward and downward. The effective operator of interaction between magnetoexcitons is written as

$$H_{int} = \frac{1}{2S}\sum_{\mathbf{p}_1+\mathbf{p}_2=\mathbf{p}_3+\mathbf{p}_4} \left[U_+(a^+_{\mathbf{p}_4} a^+_{\mathbf{p}_3} a_{\mathbf{p}_2} a_{\mathbf{p}_1} + b^+_{\mathbf{p}_4} b^+_{\mathbf{p}_3} b_{\mathbf{p}_2} b_{\mathbf{p}_1}) - U_- a^+_{\mathbf{p}_4} b^+_{\mathbf{p}_3} a_{\mathbf{p}_2} b_{\mathbf{p}_1}\right], \quad (28)$$

where U_+ and U_- are two-dimensional Fourier transforms of $U_+(R)$ and $U_-(R)$ at $\mathbf{p} = 0$ and S is the area of the system. We note that the classical turning point of the dipole–dipole interaction is a suitable cutoff parameter for the Fourier transformation. We also note that the cutoff parameter is much higher for the potential $U_+(R)$ than for $U_-(R)$. We can therefore state that $U_+ > 0$, $U_- < 0$, and $|U_-| > |U_+|$.

We apply the Bogolyubov approximation at $T = 0$ and assume that $(N - N_0)/N_0 \ll 1$, where N is the total number of particles and N_0 is the number of particles in the condensate. The Bogolyubov approximation ignores the interaction between above-condensate particles and accounts for the interaction between the particles of the condensate and between above-condensate particles and those of the condensate. The total Hamiltonian then becomes

$$\begin{aligned} H_{tot} = \frac{1}{2}\sum_{\mathbf{p}\neq 0} \Big\{ &\left[\epsilon_0(p) + (U_+ + U_-)\, n\right] \\ &\times (a^+_{\mathbf{p}} a_{\mathbf{p}} + b^+_{\mathbf{p}} b_{\mathbf{p}} + a^+_{-\mathbf{p}} a_{-\mathbf{p}} + b^+_{-\mathbf{p}} b_{-\mathbf{p}}) \\ &+ 2U_+ n(a^+_{\mathbf{p}} a^+_{-\mathbf{p}} + a_{\mathbf{p}} a_{-\mathbf{p}} + b^+_{-\mathbf{p}} b^+_{\mathbf{p}} + b_{-\mathbf{p}} b_{\mathbf{p}}) \\ &+ U_- n(a^+_{\mathbf{p}} b^+_{-\mathbf{p}} + a_{\mathbf{p}} b_{-\mathbf{p}} + a^+_{-\mathbf{p}} b^+_{\mathbf{p}} + a_{-\mathbf{p}} b_{\mathbf{p}} \\ &+ a^+_{\mathbf{p}} b_{\mathbf{p}} + a^+_{-\mathbf{p}} b_{-\mathbf{p}} + a_{\mathbf{p}} b^+_{\mathbf{p}} + a_{-\mathbf{p}} b^+_{-\mathbf{p}}) \Big\}. \end{aligned} \quad (29)$$

We diagonalize the total Hamiltonian using a unitary transformation of the Bogolyubov type [99]:

$$a_{\mathbf{p}} = \frac{\alpha_{\mathbf{p}} + A_{\mathbf{p}}\alpha^{+}_{-\mathbf{p}} + B_{\mathbf{p}}\beta^{+}_{-\mathbf{p}} + C_{\mathbf{p}}\beta_{\mathbf{p}}}{(1 - A^2_{\mathbf{p}} - B^2_{\mathbf{p}} - C^2_{\mathbf{p}})^{1/2}} ,$$

$$b_{\mathbf{p}} = \frac{\beta_{\mathbf{p}} + A_{\mathbf{p}}\beta^{+}_{-\mathbf{p}} + B_{\mathbf{p}}\alpha^{+}_{-\mathbf{p}} + C_{\mathbf{p}}\alpha_{\mathbf{p}}}{(1 - A^2_{\mathbf{p}} - B^2_{\mathbf{p}} - C^2_{\mathbf{p}})^{1/2}} ,$$

where the coefficients $A_{\mathbf{p}}$, $B_{\mathbf{p}}$, and $C_{\mathbf{p}}$ are found from the condition that the coefficients with nondiagonal terms in the Hamiltonian vanish. This gives

$$H_{\text{tot}} = \sum_{\mathbf{p}\neq 0} \epsilon(p)(\alpha^{+}_{\mathbf{p}}\alpha_{\mathbf{p}} + \beta^{+}_{\mathbf{p}}\beta_{\mathbf{p}}) ,$$

with the quasiparticle spectrum

$$\epsilon_1^2(p) = \epsilon_0^2(p) + 2nU_+\epsilon_0(p) ,$$

$$\epsilon_2^2(p) = \epsilon_0^2(p) + 2n(U_+ + U_-)\,\epsilon_0(p).$$

Because $U_+ > 0$ and $U_- < 0$, it follows that $p > 0$ for $\epsilon_1^2(p) > \epsilon_2^2(p)$. Therefore, only quasiparticles with the spectrum $\epsilon_2^2(p)$ are excited, because their excitation requires lower energy than that of quasiparticles with the spectrum $\epsilon_1^2(p)$. Because $U_+ + U_- < 0$, we easily see from (4) that the excitation spectrum becomes purely imaginary at low momenta $p < \sqrt{4Mn|U_+ + U_-|}$. This means that the system of weakly interacting indirect magnetoexcitons in a superlattice is unstable. This instability is enhanced as the magnetic field strength H increases, because this results in an increase in the magnetic mass M and therefore expands the range of p in which the energy of collective excitations is purely imaginary.

We now consider the ground state of a weakly nonideal Bose gas of magnetobiexcitons formed by pairs of antiparallel magnetoexcitons located in neighboring pairs of graphene layers (Fig. 6). If the binding energy of a magnetobiexciton is much lower than the binding energy of its constituent magnetoexcitons and the magnetobiexciton radius is much larger than the size of the magnetoexciton, then we can use the adiabatic approximation and regard magnetoexcitons as structureless particles. The applicability condition for this approximation is established below. As follows from the approximations used above, D is greater than the size of a magnetoexciton, and therefore the potential energy of interaction between magnetoexcitons at a distance r has the form

$$U(r) = \frac{e^2}{\varepsilon r} - \frac{2e^2}{\varepsilon(r^2 + D^2)^{1/2}} + \frac{e^2}{\varepsilon(r^2 + 4D^2)^{1/2}} . \qquad (30)$$

Magnetoexcitons are attracted for $r > 1.11D$ and repulsed for $r < 1.11D$. The potential energy minimum lies at $r = r_0 \approx 1.67D$.

To calculate the parameters of the magnetobiexciton, we consider the problem of a bound state of two magnetoexcitons in their center-of-mass reference frame. For estimates, we approximate the potential well in the neighborhood r_0 by a rectangular potential well of the depth $V_0 = 0.04e^2/(\varepsilon D)$ and width $a = 2D$, as shown in Fig. 7. If the wave function of the relative motion is written as $\psi(r, \varphi) = \exp(\mathrm{i}m\varphi)f(r)/\sqrt{r}$, where m is the relative orbital motion, then the function $f(r)$ obeys the one-dimensional Schrödinger equation for a particle with the equivalent mass $\mu = M/2$ placed in the above square potential well (see Fig. 7) and in an additional centrifugal potential $U_{\text{cf}}(r) = \hbar^2(m^2 - 1/4)/(2\mu r^2)$. Because the dimensionless parameter $2\mu V_0 a^2/\hbar^2 = 0.32(D/l_H)^4$ that characterizes the properties of the well is much greater than unity for $D \gg l_H$, it is possible to show that a large number of bound states exist in this well (if we ignore the centrifugal potential). The ground state energy then equals $E = -V_0 + \pi^2 e^2 l_H^4/(8\varepsilon D^5) \approx -V_0$. We can neglect the centrifugal potential because its value inside the well is of the order of $e^2 l_H^4/(\varepsilon D^5)$ and is much lower than the binding energy $|E|$.

The binding energy of a magnetoexciton for $D \gg l_H$ is thus approximately equal to $0.04e^2/(\varepsilon D)$ and the characteristic 'size' of its wave function is of the order of $a \sim D$, while the binding energy of constituent magnetoexcitons equals $e^2/(\varepsilon D)$ and the radii are of the order of l_H. The adiabatic approximation is therefore valid for $D \gg l_H$.

The magnetobiexciton discussed above has the nonzero quadrupole moment $Q_0 = 2eD^2$ (the larger axis of the quadrupole is perpendicular to the plane of the graphene layers). Hence, indirect magnetobiexcitons interact at distances $R \gg D$ as repulsive quadrupoles aligned in parallel: $U(R) = 9e^2D^4/(\varepsilon R^5)$. Using the theory of the two-dimensional Bose gas [74, 94] as in Section 6, we calculate the potential μ of magnetobiexcitons in the ladder approxima-

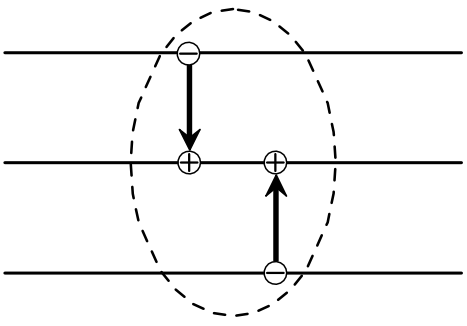

Figure 6. Schematic diagram of the structure of a quasi-two-dimensional indirect magnetobiexciton composed of two antiparallel indirect magnetoexcitons located in two neighboring pairs of graphene layers.

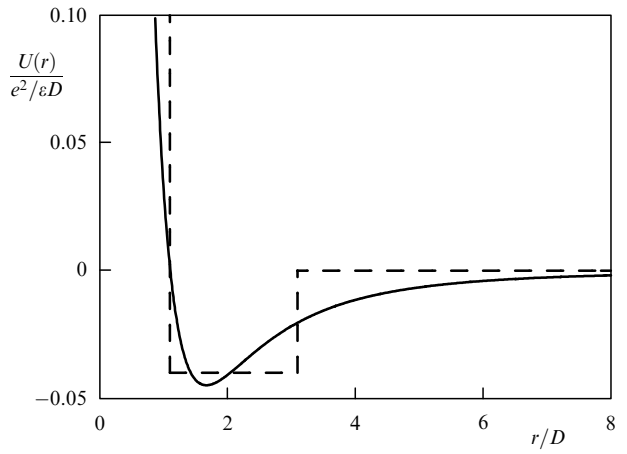

Figure 7. Interaction potential (30) of two magnetoexcitons aligned in an antiparallel manner (solid curve) and the square potential well approximating it (dashed line).

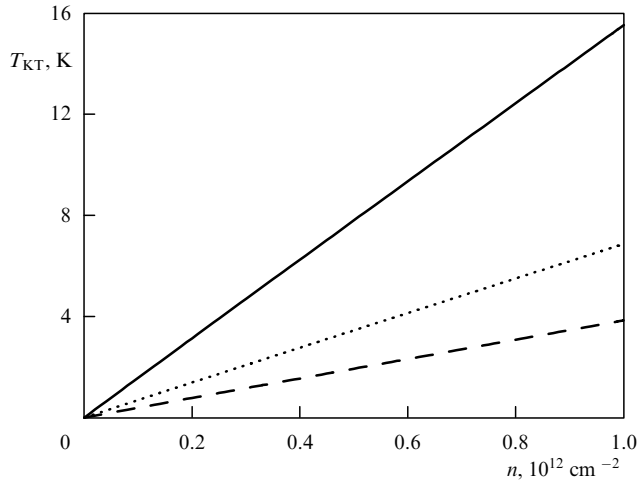

Figure 8. The Kosterlitz – Thouless transition temperature as a function of the magnetoexciton concentration in the structure of three graphene layers separated by SiO_2 layers ($\varepsilon \approx 4.5$) $D = 10$ nm thick. The magnetic field B is 10 T (solid line), 15 T (dotted line), and 20 T (dashed line).

tion:

$$\mu = \frac{4\pi\hbar^2 n_{\rm bex}}{M_{\rm bex} \ln\left\{\hbar^{4/3}\varepsilon^{2/3}/[8\pi(9M_{\rm bex}e^2D^4)^{2/3}n_{\rm bex}]\right\}}, \qquad (31)$$

where $n_{\rm bex} = n/2$ is the magnetobiexciton density and $M_{\rm bex} = 2M$ is their mass. The collective spectrum of excitations of the system of magnetobiexcitons has an acoustic form $\epsilon(p) = c_s p$ ($c_s = \sqrt{\mu/M_{\rm bex}}$ is the speed of sound) and satisfies the Landau superfluidity criterion. To evaluate the density of the superfluid component and the temperature of the Kosterlitz – Thouless transition to the superfluid state, we can use formulas (26) and (27) with the substitutions $n \to n_{\rm bex}$, $M \to M_{\rm bex}$ and with the speed of sound corresponding to chemical potential (31). $T_{\rm KT}$ as a function of the magnetoexciton concentration at different magnetic field strengths is plotted in Fig. 8.

Therefore, the exciton line in the above three-layer structure may disappear at low temperatures, while the magnetobiexciton line may survive. As in the system of magnetoexcitons studied in Section 6, the temperature of the Kosterlitz – Thouless transition to the superfluid state at a fixed density of magnetobiexcitons decreases as the magnetic field strength and the interlayer separation increase, owing to the increasing magnetic mass. The temperature $T_{\rm KT}$ decreases as H^{-2} for $D \gg l_H$. The repulsion between magnetobiexcitons ensures the stability of the system.

8. Superfluid state of the system of composite fermions in a graphene bilayer

As in Section 6, we consider an electron – hole bilayer — two electrode-controlled barrier-separated graphene planes (see Fig. 4) placed in a strong magnetic field; however, the control parameters (the magnetic field H and the chemical potential $\mu_1 = \mu_2$ or $\mu_1 = -\mu_2$) are such that the filling factor of Landau levels in both graphene sheets is $\nu = 1/2$. This system is largely similar to the one studied experimentally by Eisenstein's group [100] — an electron bilayer in a semiconductor (the difference stems from the spinor nature of the electron wave function in graphene, the presence of the Berry phase, etc). With one-half filling factor, it is convenient to apply the Halperin – Lee – Reed gauge transformation [101] and pass to the composite-fermion representation [102], which essentially means the following. The filling $\nu = 1/2$ corresponds to two magnetic flux quanta per electron. By assigning two flux quanta to each electron (which corresponds to the Halperin – Lee – Reed gauge transformation), we obtain new quasiparticles, composite fermions.

In the mean-field approximation, that is, with the flux quanta 'tied' to electrons uniformly 'smeared,' the magnetic field leaves electrons unaffected. Therefore, both layers contain Fermi spheres of composite electrons (or, by virtue of the electron – hole symmetry, Fermi spheres of composite holes). It can be shown [103] that composite electrons of different layers undergo an effective repulsion, while the composite electrons of one layer are attracted to the composite holes of another layer. This creates a situation similar to the one treated in Section 5 with no magnetic field: the electron – hole pairing arises between the layers and a superfluid system of pairs of composite fermions is formed in a graphene bilayer (both when the chemical potentials of the layers are identical and when they have opposite signs).

9. Magnetoplasmons in graphene-based layered structures

In this section, we present some results concerning the properties of magnetoplasmons in one-layer graphene, in a graphene bilayer, and in a superlattice of graphene layers (see [104]). Magnetoplasmons are collective electron oscillations whose dispersion relation $\epsilon(q)$ satisfies the equation $\varepsilon(q, \epsilon(q)) = 0$, where $\varepsilon(q, \omega)$ is the dynamic dielectric permittivity that determines the effective interaction between electrons in graphene.

In the random-phase approximation, the dielectric permittivity is $\varepsilon(q, \omega) = 1 - v(q)\,\Pi(q, \omega)$, where $v(q) = 2\pi e^2/(\varepsilon_b q)$ is the bare Coulomb interaction, ε_b is the dielectric permittivity of the ambient medium, and $\Pi(q, \omega)$ is the polarization operator. Using the explicit form of the electron wave functions in one-layer graphene in a magnetic field (given, e.g., in [87]), we find that

$$\Pi(q, \omega) = \frac{g_s g_v}{2\pi l_H^2} \sum_{n,n'} \frac{f_n - f_{n'}}{\hbar\omega + \epsilon_n - \epsilon_{n'} + i\delta} F_{n,n'}(q) \qquad (32)$$

in the linear response approximation, where $\delta \to 0^+$, $\epsilon_n = {\rm sgn}(n)\,\hbar v_F \sqrt{2|n|}/l_H$ is the energy of the nth Landau level ($n = 0, \pm 1, \pm 2, \ldots$), and f_n is the filling factor of this level. The overlapping coefficient $F_{n,n'}(q)$ of levels n and n' is given by

$$F_{n,n'}(q) = \frac{2^{\delta_{n,0}+\delta_{n',0}-2}}{[(|n| - |n'|)!]^2} \left[-\frac{q^2 l_H^2}{2}\right]^{|n|-|n'|} \times \left[{\rm sgn}(n)\,{\rm sgn}(n')\,\frac{(|n|-1)!}{(|n'|-1)!} + \frac{|n|!}{|n'|!}\right].$$

If $T = 0$, the highest Landau level and all lower levels are completely filled, while the remaining levels are empty. In our calculations, only the transitions between the five lowest Landau levels of the conduction band and the five highest levels of the valence band were taken into account. Figure 9 plots the solutions of the dispersion equation in one-layer graphene that correspond to real frequencies (horizontal lines

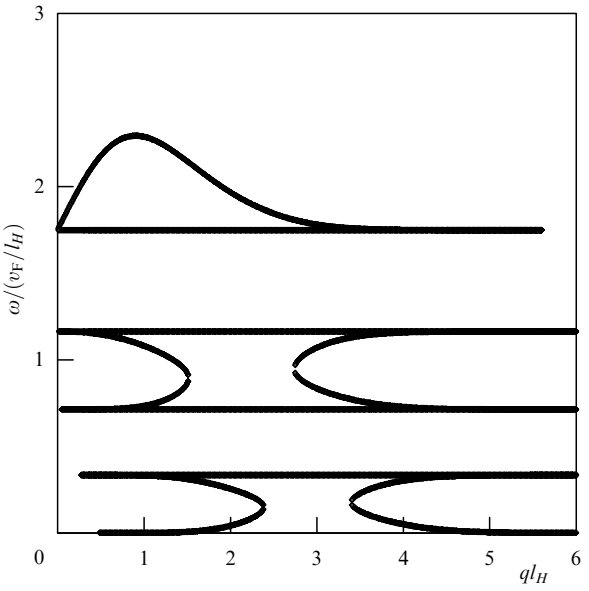

Figure 9. Dispersion relations for magnetoplasmons in one-layer graphene (solutions with real frequencies).

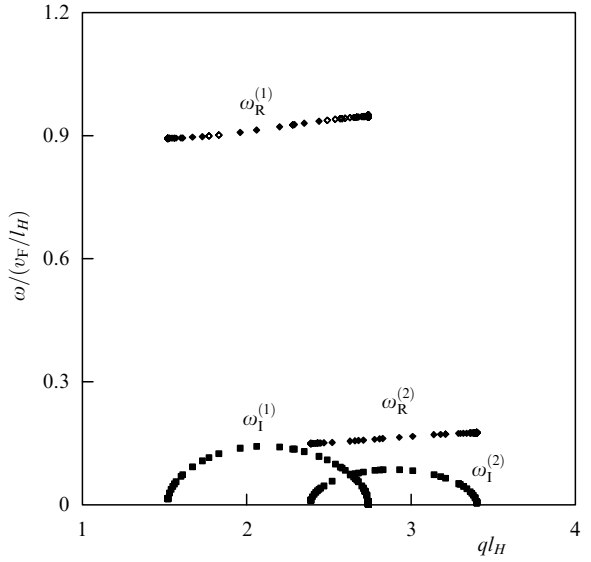

Figure 10. Real (ω_R) and imaginary (ω_1) components of the magnetoplasmon frequency in one-layer graphene (solutions with complex frequencies).

correspond to one-particle transitions between Landau levels). In this case, magnetoplasmons are self-sustained oscillations; however, having reached the region of one-particle electron – hole excitations, they acquire a finite lifetime through Landau damping (a decay of the plasmon to electron – hole pairs or, as Ginzburg showed more clearly, through the inverse Vavilov – Cherenkov effect). Figure 10 shows solutions of the dispersion equation that correspond to complex frequencies.

The decaying magnetoplasmon modes have the real component of the frequency linear in q and exist in those regions of q where the group velocity of nondecaying magnetoplasmons is negative. Negative group velocity at $ql_H > 1$ arises as a response to the magnetic field [105]. We repeated the calculations for dispersion curves shown in Fig. 9 using a larger number of Landau levels in both bands. This brought no qualitatively different results, except for a larger number of one-particle excitation lines. However, lower branches of collective excitations change insignificantly.

We now consider magnetoplasmons in two-layer graphene for which the electron Hamiltonian has form (9). The explicit form of the electron wave functions in a magnetic field is given in [55] and the energies of Landau levels are $\epsilon_n^{(b)} = \mathrm{sgn}(n)\,\hbar\omega_c\sqrt{|n|(|n|-1)}$, where $n = 0, 1, \pm 2, \pm 3, \ldots$, $\omega_c = eH/(m^*c)$, $m^* = 0.033m_e$. The polarization operator of two-layer graphene is calculated using (32) and the substitution $\epsilon_n \to \epsilon_n^{(b)}$, as well as the following expression for the overlapping integral:

$$F_{n,n'}^{(b)}(q) = 2^{\delta_{n,0}+\delta_{n,1}+\delta_{n',0}+\delta_{n',1}-2} \times \left\{ \left| \int \mathrm{d}x \exp(\mathrm{i}xq_x)\, \Phi_{|n|}(x)\Phi_{|n'|}(x + l_H^2 q_y) \right|^2 + \mathrm{sgn}(n) \times \mathrm{sgn}(n') \left| \int \mathrm{d}x \exp(\mathrm{i}xq_x)\Phi_{|n|-2}(x)\Phi_{|n'|-2}(x + l_H^2 q_y) \right|^2 \right\}.$$

Here, $\Phi_n(x) = (2^n n!\sqrt{\pi} l_H)^{-1/2} \exp[-x^2/(2l_H^2)]\, H_n(x/l_H)$ is the eigenfunction of the one-dimensional oscillator and H_n is the Hermite polynomial.

The solutions of the dispersion equation for two-layer graphene that correspond to nondecaying plasmon modes are plotted in Fig. 11. As in one-layer graphene, the magnetic field makes the group velocity negative for a number of values of wave vectors. Energy transfer between electrons and collective excitations occurs only when the phase velocity of the collective mode equals the velocity of one of the electrons.

The dispersion equation for a graphene bilayer in which tunneling between layers separated by a distance D is negligible has the form [76, 106]

$$v(p)\,\Pi(q,\omega)\left[1 - \exp(-2qD)\right] - 1 = \pm\exp(-qD), \quad (33)$$

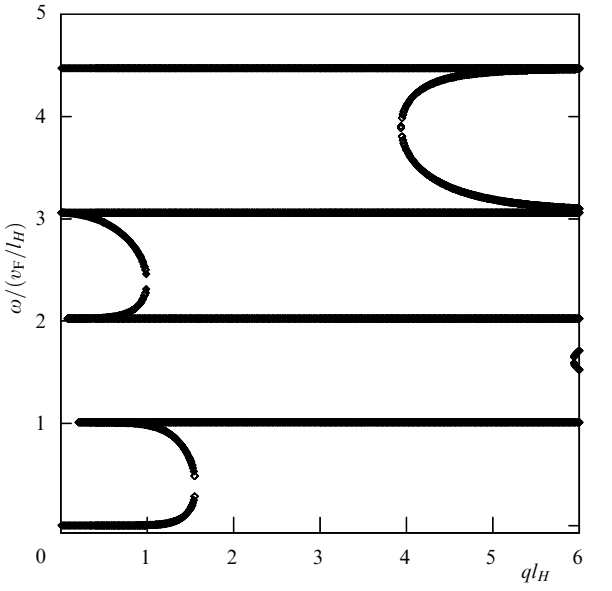

Figure 11. Real solutions of the dispersion equation for magnetoplasmons in two-layer graphene with the filling factor $\nu = 1$.

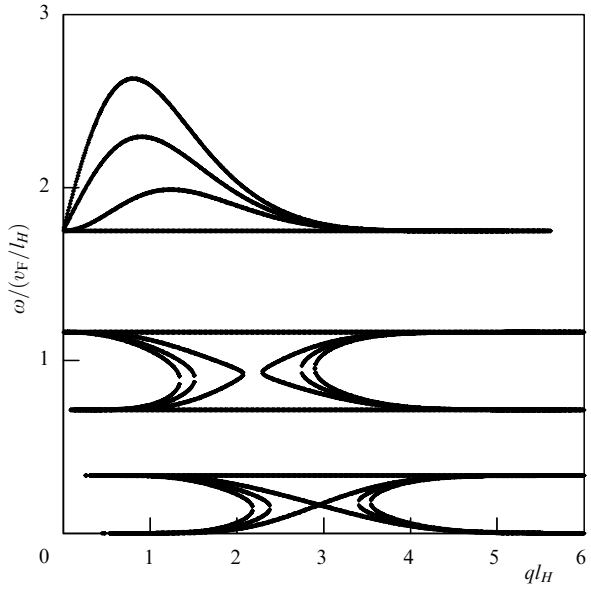

Figure 12. Real solutions of the dispersion equation for magnetoplasmons in a graphene bilayer at $D = l_H$. Only the highest Landau level in the valence band is filled.

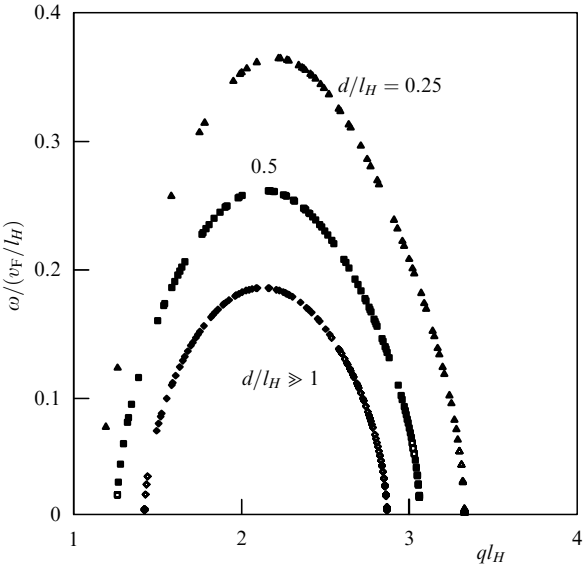

Figure 13. Imaginary part of the magnetoplasmon frequency in single-layer graphene in comparison to the results for an infinite superlattice of graphene layers at $\nu = 1$, $k_z l_H = 0.1$, and superlattice constants $D = 0.25 l_H$, $D = 0.5 l_H$, and $D \gg l_H$.

where we assumed that the polarization operator $\Pi(q, \omega)$ defined by (32) is the same for both graphene layers. The interlayer Coulomb interaction results in mixing of plasma modes of each layer, which produces two dispersion branches. Solutions of Eqn (33) with real frequencies are plotted in Fig. 12. We again see regions of magnetoplasmon decay.

Finally, we consider a superlattice composed of graphene layers parallel to the plane (x, y) and separated by a distance D along the z axis. The graphene layers are immersed into a medium with a dielectric permittivity ε_b and tunneling between layers is negligibly small. The dispersion equation for magnetoplasmons in the superlattice has the form [29, 107] $1 - v(q)\,\Pi(q, \omega)\,S(q, k_z) = 0$, where $\Pi(q, \omega)$ is the polarization operator of one graphene sheet and $S(q, k_z) = \sinh(qD)/[\cosh(qD) - \cos(k_z D)]$ is the structural factor determining the phase coherence of collective excitations in different layers. We solved the dispersion equation for the complex frequency of magnetoplasmons; the results are plotted in Fig. 13 for $k_z l_H = 0.1$ and several values of D.

The results of our numerical calculation for an infinitely large superlattice show that both magnetoplasmon modes and excitations corresponding to one-particle electron transitions between Landau levels exist. The collective mode with the highest energy has an increasing frequency for $ql_H < 1$, but undergoes Landau damping at large wave vectors. Figure 13 shows that the imaginary component of the frequency of the collective mode responsible for its damping increases in the superlattice, as compared to damping in one-layer graphene. Furthermore, by virtue of in-phase superposition of oscillations in individual layers, both the real and the imaginary frequency components sharply increase. This effect is enhanced as the ratio D/l_H decreases.

The enhanced instability of magnetoplasmons in a superlattice can be used for converting the energy of magnetoplasmon modes into electromagnetic radiation in the terahertz range. For example, the magnetoplasmon frequency in the magnetic field 10 T corresponding to the filling factor $\nu = 1$ falls into the range near 3.6 THz. An additional advantage of such radiation sources consists in the possibility of controlling the frequency of emitted radiation by changing the magnetic field strength.

10. Conclusion

Numerous theoretical and experimental results have been obtained since the experimental discovery of graphene in 2004, with several hundred papers on graphene having been published. A number of new effects have been discovered that have no analogs among other substances, and a still greater number of unusual effects have been predicted theoretically and await experimental investigation.

It would be difficult to overestimate the importance of the contribution to fundamental science brought about by studying graphene: this material allows working with massless charged fermions that have no analogs among elementary particles. Graphene is not only unique from the standpoint of its electron properties but is also the closest among all nanostructures yet produced to the ideal two-dimensional crystal, because it is just one atom thick and has a clearly expressed crystal structure. Consequently, the preparation of graphene produced two breakthroughs simultaneously: one in fundamental physics and one in the physics of nanostructures. We can look at the experimental study of the wonderful properties of graphene as the most spectacular discovery in the physics of mesoscopic systems in the last 20 years, a discovery of the same magnitude as those of the integral and fractional quantum Hall effects.

We note that in addition to graphene, Novoselov, Geim, Morozov et al. also prepared other two-dimensional crystals [9], and this opened a new field in the physics of nanostructures — the study of membranes of monatomic thickness.

We now turn to certain important aspects of the fundamental physics of graphene that still welcome research. First, these are the recently detected anomalies in the quantum Hall effect. As we mentioned in Section 3, the Hall conductivity quantization $\sigma_{xy} = \nu e^2/h$ with $\nu = \pm 2, \pm 6, \ldots$, even though it

is not typical of conventional two-dimensional systems, is explainable in terms of the single-particle ultrarelativistic dynamics of electrons in graphene. But it was discovered in [108] that new Hall steps at $\nu = 0, \pm 1, \pm 4$ are formed in strong magnetic fields ($B > 20$ T). Subsequent experiments [109] showed that splittings at $\nu = 0$ and $\nu = \pm 4$ correspond to lifting the spin degeneracy and that the widths of the corresponding gaps are proportional to $|\mathbf{B}|$, exactly as expected for the Zeeman splitting. In fact, the gap at $\nu = 0$, being located at the Dirac point, has certain specific features that distinguish it from similar Zeeman gaps at Landau levels for $n \neq 0$ [110]. As regards the gaps at $\nu = \pm 1$, they are proportional to $\sqrt{B_\perp}$, where $B_\perp$ is the field component perpendicular to the graphene plane, and this points to the many-body nature of these gaps. Therefore, sufficiently strong magnetic fields remove the degeneracy of the $n = 0$ level both in spins and in valleys: $n = 0$ corresponds to spin splitting, and $\nu = \pm 1$ to some collective electron phenomenon that breaks the valley symmetry. A number of versions of the theoretical explanation of this phenomenon have been suggested (such as the quantum Hall ferromagnetism, spontaneous mass generation, and the pairing of composite fermions), but ultimate clarity has not been achieved yet (see, e.g., [109, 111] and the references therein).

Another unsolved problem is the nature of the minimum conductivity of graphene, which, according to experimental data, equals $4e^2/h$ [10, 51] when the Fermi energy is at the Dirac point. The existence of a minimum conductivity was thought for a long time to stem from disorder (such as ripples) that creates electron – hole puddles (see, e.g., [112] and the references therein), but the theory predicts the minimum conductivity smaller by a factor of π than the experimental value. It was later shown that the same value of conductivity, obtained theoretically by considering perfectly pure graphene [113], is a characteristic property of chiral particles and thus makes it unnecessary to involve any disorder. Hence, it is necessary to clarify what roles are played in the formation of minimum conductivity by chirality, disorder, and electron – electron interactions.

The chiral nature of electrons must theoretically manifest itself in a number of quantum electrodynamics effects, which must be especially strong in graphene in view of the zero gap between the conduction and the valence bands. Thus, the relevant transport measurements [114] were carried out to study the predicted Klein tunneling across the potential barrier in graphene [44], but scattering by impurities introduced essential distortion into the results.

Optical studies of graphene are of great interest. In addition to the marvelous result on the universality of the absorption coefficient of graphene in a broad spectral range [115], which is determined by the fine structure constant α and equals $\pi\alpha$, it is interesting to directly study the damping rate of quasiparticles as a function of their energy using time-resolved spectroscopy (see, e.g., [116]). This would provide important information on the properties of the electron Fermi liquid in graphene and on possible deviations from the Landau theory [59, 68, 117].

Also unsolved are the aspects connected with the mechanical stability of graphene. Calculations in the harmonic approximation show that mean-square displacements of segments of a graphene sheet perpendicular to its plane diverge as L^2, where L is the linear size of the sheet. This points to an instability with respect to crumpling. However, taking the effects of anharmonism into account yields the function L^r with $r \approx 0.6$, which in some sense stabilizes the graphene membrane (see, e.g., [118], as well as [23] and the references therein). Experiments [11] showed that graphene is covered with slight local distortions — ripples several nanometers in size. Although numerical modeling [119] gave the same result, much about the properties of ripples remains unclear. The mechanical properties of graphene as a two-dimensional membrane need to be studied further.

We can now discuss the main areas of application-oriented research on graphene. The most actively considered nanoelectronic application of graphene is now the creation of field transistors that use the properties of graphene such as the high carrier mobility and the ease of processing and of connecting electrodes. Simple specimens of field transistors have been designed and their characteristics measured [120]. Unfortunately, leak currents are large owing to the presence of minimum conductivity, and hence the unique band structure of graphene is a hindrance for designing traditional electronic devices. To improve the characteristics of such transistors, a gap in the spectrum is needed; it may appear, for example, following a chemical modification of graphene [121] or as a result of interaction with a substrate [122]. Less conventional prototypes of possible future devices are quantum-dot-based one-electron transistors, which function using a Coulomb blockade. Owing to the specifics of the graphene band structure, distances between energy levels formed in graphene quantum dots as a result of spatial confinement are much larger than in similar devices based on other materials [14, 123]. This allows one-electron transistors to work at room temperature.

Unique properties of graphene make it an attractive candidate as a material for implementing electronic devices that differ dramatically from conventional ones. For instance, graphene can be used to design the element basis of spintronics [124], in which the spin degree of freedom of electrons is employed. Very weak spin – orbit coupling and high charge mobility in graphene allow spin transport at submicron distances at room temperatures [125]. An additional (valley) degree of freedom for electrons in graphene can also be used for signal transfer. Valley degeneration can be removed under certain conditions, after which valley polarization can be generated and detected [126].

Graphene as a two-dimensional material may be valuable not only for electronic applications. We mention the storage of large quantities of hydrogen absorbed on the surface of graphene [127], the creation of new composite materials [128], and high-sensitivity graphene-based gas sensors [129]. Graphene can also be used as an almost transparent electrode in liquid-crystal indicators [130] and as a nanomechanical resonator permitting detection of ultrasmall masses [131]. The constancy of the optical absorption coefficient of graphene in a broad spectral range makes it useful for creating optically neutral coatings and detectors of electromagnetic radiation (as stacks of noncontiguous graphene sheets) whose sensitivity would be independent of the wavelength in the range from terahertz to far-infrared frequencies [16]. Of course, this is the right moment to recall Niels Bohr's maxim, "Prediction is very difficult, especially about the future." Prospects for technological applications of graphene are thus greatly dependent on whether its manufacturing becomes manageable and economical.

It must be emphasized that graphene holds enormous potential for building various structures whose properties

may greatly differ from those of the initial graphene. Chemical modification may change the geometry [132] and electronic properties [121] of a graphene sheet. It is also possible to create various superlattices on graphene sheets in order to modify its band structure. Such superlattices can be created by controlled atomic adsorption [15], by lithographic techniques [133], or by external fields [134].

The original results presented in this talk show that graphene and graphene-based nanostructures are very interesting subjects for implementing superfluidity and other coherent effects. High quality and the possibility of manufacturing compact multilayer systems are bases for expecting that collective effects will be easier to observe in them than in traditional quasi-two-dimensional systems. A specific feature of graphene, its linear dispersion, leads to new relations between the kinetic and potential energies of a system of electrons and thus opens ways of implementing new regimes of behavior of quantum systems.

Yu E L is grateful to O L Berman, D K Efimkin, G Gambs, and R Ya Kezerashvili for their collaboration and to Yu V Kopaev for the useful discussions. The work was supported by RFBR and RAS Presidium grants. A A S is grateful for support to the Dynasty Foundation for Noncommercial Programs and to the Russian Science Support Foundation.

References

1. Lozovik Yu E, Popov A M *Usp. Fiz. Nauk* **177** 786 (2007) [*Phys. Usp.* **50** 749 (2007)]; Saito R, Dresselhaus G, Dresselhaus M S (Eds) *Physical Properties of Carbon Nanotubes* (London: Imperial College Press, 1998)
2. Lozovik Yu E, Popov A M *Usp. Fiz. Nauk* **167** 751 (1997) [*Phys. Usp.* **40** 717 (1997)]
3. Dresselhaus M S, Dresselhaus G *Adv. Phys.* **51** 1 (2002)
4. Peierls R E *Ann. Inst. Henri Poincaré* **5** 177 (1935); Landau L D *Phys. Z. Sowjetunion* **11** 26 (1937)
5. Berezinskii V L *Nizkotemperaturnye Svoistva Dvumernykh Sistem s Nepreryvnoi Gruppoi Simmetrii* (Low-temperature properties of systems with continuous symmetry group) (Moscow: Fizmatlit, 2007)
6. Kosterlitz J M, Thouless D J *J. Phys. C: Solid State Phys.* **6** 1181 (1973); Nelson D R, Kosterlitz J M *Phys. Rev. Lett.* **39** 1201 (1977)
7. Nelson D R, Halperin B I *Phys. Rev. B* **19** 2457 (1979)
8. Novoselov K S, Geim A K, Morozov S V, Jiang D, Zhang Y, Dubonos S V, Grigorieva I V, Firsov A A *Science* **306** 666 (2004)
9. Novoselov K S et al. *Proc. Natl. Acad. Sci. USA* **102** 10451 (2005)
10. Novoselov K S, Geim A K, Morozov S V, Jiang D, Katsnelson M I, Grigorieva I V, Dubonos S V, Firsov A A *Nature* **438** 197 (2005)
11. Meyer J C et al. *Nature* **446** 60 (2007)
12. Ferrari A C et al. *Phys. Rev. Lett.* **97** 187401 (2006); Gupta A et al. *Nano Lett.* **6** 2667 (2006)
13. de Heer W A et al. *Solid State Commun.* **143** 92 (2007)
14. Özyilmaz B et al. *Appl. Phys. Lett.* **91** 192107 (2007)
15. Chernozatonskii L A, Sorokin P B, Brüning J W, arXiv:0709.1015
16. Lozovik Yu E, Merkulova S P (to be published)
17. Morozov S V et al. *Phys. Rev. Lett.* **100** 016602 (2008); Bolotin K I et al. *Solid State Commun.* **146** 351 (2008); Garcia N et al., arXiv:0803.2203
18. Novoselov K S et al. *Science* **315** 1379 (2007)
19. Wallace P R *Phys. Rev.* **71** 622 (1947)
20. Katsnelson M I, Novoselov K S *Solid State Commun.* **143** 3 (2007)
21. Katsnelson M I *Mater. Today* **10** (1–2) 20 (2007)
22. Geim A K, Novoselov K S *Nature Mater.* **6** 183 (2007)
23. Castro Neto A H et al., arXiv:0709.1163
24. Slonczewski J C, Weiss P R *Phys. Rev.* **109** 272 (1958)
25. McClure J W *Phys. Rev.* **108** 612 (1957)
26. Painter G S, Ellis D E *Phys. Rev. B* **1** 4747 (1970)
27. Dresselhaus M S, Dresselhaus G *Adv. Phys.* **30** 139 (1981)
28. DiVincenzo D P, Mele E J *Phys. Rev. B* **29** 1685 (1984)
29. Shung K W-K *Phys. Rev. B* **34** 979 (1986)
30. Shung K W-K *Phys. Rev. B* **34** 1264 (1986)
31. Fradkin E *Phys. Rev. B* **33** 3257 (1986)
32. Haldane F D M *Phys. Rev. Lett.* **61** 2015 (1988)
33. Semenoff G W *Phys. Rev. Lett.* **53** 2449 (1984)
34. Bogolyubov N N, Shirkov D V *Vvedenie v Teoriyu Kvantovannykh Polei* (Introduction to the Theory of Quantized Fields) 4th ed. (Moscow: Nauka, 1984) [Translated into English (New York: John Wiley, 1980)]
35. Volkov B A, Idlis B G, Usmanov M Sh *Usp. Fiz. Nauk* **165** 799 (1995) [*Phys. Usp.* **38** 761 (1995)]
36. Gusynin V P, Sharapov S G, Carbotte J P *Int. J. Mod. Phys. B* **21** 4611 (2007)
37. Kawamura K, Brown R A *Phys. Rev. B* **37** 3932 (1988)
38. Gusynin V P, Sharapov S G *Phys. Rev. Lett.* **95** 146801 (2005)
39. Bostwick A et al. *Nature Phys.* **3** 36 (2007)
40. McChesney J L et al., arXiv:0705.3264
41. Bostwick A et al. *New J. Phys.* **9** 385 (2007)
42. Wu X et al. *Phys. Rev. Lett.* **98** 136801 (2007)
43. Morozov S V et al. *Phys. Rev. Lett.* **97** 016801 (2006); Tikhonenko F V et al. *Phys. Rev. Lett.* **100** 056802 (2008)
44. Katsnelson M I, Novoselov K S, Geim A K *Nature Phys.* **2** 620 (2006)
45. Beenakker C W J, arXiv:0710.3848
46. Ando T, Nakanishi T, Saito R *J. Phys. Soc. Jpn.* **67** 2857 (1998)
47. Nomura K, Koshino M, Ryu S *Phys. Rev. Lett.* **99** 146806 (2007)
48. Silvestrov P G, Efetov K B *Phys. Rev. Lett.* **98** 016802 (2007); Matulis A, Peeters F M *Phys. Rev. B* **77** 115423 (2008)
49. Pereira V M et al. *Phys. Rev. Lett.* **96** 036801 (2008)
50. De Martino A, Dell'Anna L, Egger R *Phys. Rev. Lett.* **98** 066802 (2007); Chen H-Y, Apalkov V, Chakraborty T *Phys. Rev. Lett.* **98** 186803 (2007)
51. Tan Y-W et al. *Phys. Rev. Lett.* **99** 246803 (2007)
52. Akhiezer A I, Berestetskii V B *Kvantovaya Elektrodinamika* (Quantum Electrodynamics) 4th ed. (Moscow: Nauka, 1981) [Translated into English (New York: Intersci. Publ., 1965)]
53. Fogler M M, Novikov D S, Shklovskii B I *Phys. Rev. B* **76** 233402 (2007)
54. Shytov A V, Katsnelson M I, Levitov L S *Phys. Rev. Lett.* **99** 236801, 246802 (2007)
55. McCann E, Fal'ko V I *Phys. Rev. Lett.* **96** 086805 (2006)
56. Novoselov K S et al. *Nature Phys.* **2** 177 (2006)
57. McCann E *Phys. Rev. B* **74** 161403(R) (2006)
58. Oostinga J B et al. *Nature Mater.* **7** 151 (2007)
59. González J, Guinea F, Vozmediano M A H *Nucl. Phys. B* **424** 595 (1994)
60. Mishchenko E G *Phys. Rev. Lett.* **98** 216801 (2007)
61. Hwang E H, Das Sarma S *Phys. Rev. B* **75** 205418 (2007)
62. Katsnelson M I *Phys. Rev. B* **74** 201401(R) (2006)
63. Keldysh L V, Kopaev Yu V *Fiz. Tverd. Tela* **6** 2791 (1964) [*Sov. Phys. Solid State* **6** 2219 (1965)]; Guseinov R R, Keldysh L V *Zh. Eksp. Teor. Fiz.* **63** 2255 (1972) [*Sov. Phys. JETP* **36** 1193 (1973)]
64. Khveshchenko D V *Phys. Rev. Lett.* **87** 246802 (2001); Herbut I F *Phys. Rev. Lett.* **97** 146401 (2006); Son D T *Phys. Rev. B* **75** 235423 (2007)
65. Dahal H P et al. *Phys. Rev. B* **74** 233405 (2006)
66. Zhang C-H, Joglekar Y N *Phys. Rev. B* **75** 245414 (2007)
67. Lozovik Yu E, Yudson V I *Pis'ma Zh. Eksp. Teor. Fiz.* **22** 26 (1975) [*JETP Lett.* **22** 11 (1975)]
68. González J, Guinea F, Vozmediano M A H *Phys. Rev. B* **59** R2474 (1999)
69. Barlas Y et al. *Phys. Rev. Lett.* **98** 236601 (2007); Roldán R, López-Sancho M P, Guinea F *Phys. Rev. B* **77** 115410 (2008)
70. Lerner I V, Lozovik Yu E *Zh. Eksp. Teor Fiz.* **78** 1167 (1980) [*Sov. Phys. JETP* **51** 588 (1980)]
71. Lerner I V, Lozovik Yu E *Zh. Eksp. Teor. Fiz.* **80** 1488 (1981) [*Sov. Phys. JETP* **53** 763 (1981)]; *J. Low Temp. Phys.* **38** 333 (1980)
72. Lozovik Yu E, Sokolik A A *Pis'ma Zh. Eksp. Teor. Fiz.* **87** 61 (2008) [*JETP Lett.* **87** 55 (2008)]
73. Bardeen J, Cooper L N, Schrieffer J R *Phys. Rev.* **108** 1175 (1957)
74. Lozovik Yu E, Yudson V I *Pis'ma Zh. Eksp. Teor. Fiz.* **22** 556 (1975) [*JETP Lett.* **22** 274 (1975)]; *Solid State Commun.* **19** 391 (1976); *Zh. Eksp. Teor. Fiz.* **71** 738 (1976) [*Sov. Phys. JETP* **44** 389 (1976)];

Lozovik Yu E, Nishanov V N, in *Vsesoyuz. Soveshchanie po Dielektricheskoi Elektronike, Tashkent 1973. Tezisy Dokladov* (All-Union Conf. on Dielectric Electronics) (Tashkent: Fan, 1973) p. 70
75. Lozovik Yu E, Berman O L *Pis'ma Zh. Eksp. Teor. Fiz.* **64** 526 (1996) [*JETP Lett.* **64** 573 (1996)]; *Zh. Eksp. Teor. Fiz.* **111** 1879 (1997) [*JETP* **84** 1027 (1997)]
76. Das Sarma S, Madhukar A *Phys. Rev. B* **23** 805 (1981)
77. Wunsch B et al. *New J. Phys.* **8** 318 (2006)
78. Nozières P, Schmitt-Rink S *J. Low Temp. Phys.* **59** 195 (1985)
79. Kopnin N B, Sonin E B, arXiv:0803.3772
80. Min H et al., arXiv:0802.3462
81. Lozovik Yu E, Efimkin D K (to be published)
82. Adam S et al. *Proc. Natl. Acad. Sci. USA* **104** 18392 (2007)
83. Conti S, Vignale G, MacDonald A H *Phys. Rev. B* **57** R6846 (1998)
84. Lozovik Yu E, Nikitkov M V *Zh. Eksp. Teor. Fiz.* **116** 1440 (1999) [*JETP* **89** 775 (1999)]
85. Lozovik Yu E, Poushnov A V *Phys. Lett. A* **228** 399 (1997)
86. Balatsky A V, Joglekar Y N, Littlewood P B *Phys. Rev. Lett.* **93** 266801 (2004)
87. Iyengar A et al. *Phys. Rev. B* **75** 125430 (2007)
88. Berman O L, Lozovik Yu E, Gumbs G *Phys. Rev. B* **77** 155433 (2008)
89. Gorkov L P, Dzyaloshinskii I E *Zh. Eksp. Teor. Fiz.* **53** 717 (1967) [*Sov. Phys. JETP* **26** 449 (1968)]
90. Lozovik Yu E, Ruvinsky A M *Phys. Lett. A* **227** 271 (1997)
91. Lozovik Yu E, Ruvinskii A M *Zh. Eksp. Teor. Fiz.* **112** 1791 (1997) [*JETP* **85** 979 (1997)]
92. Lozovik Yu E, Berman O L, Willander M *J. Phys.: Condens. Matter* **14** 12457 (2002)
93. Griffin A *Excitations in a Bose-Condensed Liquid* (Cambridge: Cambridge Univ. Press, 1993)
94. Lozovik Yu E, Yudson V I *Physica A* **93** 493 (1978)
95. Lozovik Yu E, Berman O L, Tsvetus V G *Phys. Rev. B* **59** 5627 (1999)
96. Lifshitz E M, Pitaevskii L P *Statisticheskaya Fizika* (Statistical Physics) (Moscow: Nauka, 1978) Vol. 2 [Translated into English (Oxford: Pergamon Press, 1980)]
97. Berman O L, Kezerashvili R Ya, Lozovik Yu E, arXiv:0711.0976
98. Berman OL, Kezerashvili R Ya, Lozovik Yu E *Phys. Rev. B* **78** 035135 (2008), arXiv:0801.1094
99. Moskalenko S A et al. *Phys. Rev. B* **66** 245316 (2002)
100. Eisenstein J P, MacDonald A H *Nature* **432** 691 (2004)
101. Halperin B I, Lee P A, Read N *Phys. Rev. B* **47** 7312 (1993)
102. Heinonen O (Ed.) *Composite Fermions: A Unified View of the Quantum Hall Regime* (Singapore: World Scientific, 1998)
103. Lozovik Yu E, Prokhorenko D V (to be published)
104. Berman O L, Lozovik Yu E, Gumbs G *Phys. Rev. B* **78** 085401 (2008)
105. Chiu K W, Quinn J J *Phys. Rev. B* **9** 4724 (1974)
106. Eguiluz A et al. *Phys. Rev. B* **11** 4989 (1975)
107. Das Sarma S, Quinn J J *Phys. Rev. B* **25** 7603 (1982)
108. Zhang Y et al. *Phys. Rev. Lett.* **96** 136806 (2006)
109. Jiang Z et al. *Phys. Rev. Lett.* **99** 106802 (2007)
110. Abanin D A et al. *Phys. Rev. Lett.* **98** 196806 (2007)
111. Shibata N, Nomura K, arXiv:0803.2418
112. Cortijo A, Vozmediano M A H, arXiv:0709.2698
113. Katsnelson M I *Eur. Phys. J. B* **51** 157 (2006); Tworzydlo J et al. *Phys. Rev. Lett.* **96** 246802 (2006)
114. Huard B et al. *Phys. Rev. Lett.* **98** 236803 (2007)
115. Nair R R et al. *Science* **320** 1308 (2008); arXiv:0803.3718
116. Dobryakov A L et al. *Zh. Eksp. Teor Fiz.* **119** 309 (2001) [*JETP* **92** 267 (2001)]
117. Das Sarma S, Hwang E H, Tse W-K *Phys. Rev. B* **75** 121406(R) (2007)
118. Le Doussal P, Radzihovsky L *Phys. Rev. Lett.* **69** 1209 (1992)
119. Fasolino A, Los J H, Katsnelson M I *Nature Mater.* **6** 858 (2007); Abedpour N et al. *Phys. Rev. B* **76** 195407 (2007)
120. Chen Z et al. *Physica E* **40** 228 (2007); Lemme M C et al. *IEEE Electron Device Lett.* **28** 282 (2007)
121. Echtermeyer T J et al., arXiv:0712.2026
122. Zhou S Y et al. *Nature Mater.* **6** 770 (2007)
123. Stampfer C et al. *Appl. Phys. Lett.* **92** 012102 (2008); Ponomarenko L A et al. *Science* **320** 356 (2008)
124. Žutić I, Fabian J, Das Sarma S *Rev. Mod. Phys.* **76** 323 (2004)
125. Hill E W et al. *IEEE Trans. Magn.* **42** 2694 (2006); Ohishi M et al. *Jpn. J. Appl. Phys.* **46** L605 (2007); Cho S, Chen Y-F, Fuhrer M S *Appl. Phys. Lett.* **91** 123105 (2007)
126. Xiao D, Yao W, Niu Q *Phys. Rev. Lett.* **99** 236809 (2007); Yao W, Xiao D, Niu Q *Phys. Rev. B* **77** 235406 (2008); Rycerz A *Phys. Status Solidi A* **205** 1281 (2008)
127. Boukhvalov D W, Katsnelson M I, Lichtenstein A I *Phys. Rev. B* **77** 035427 (2008)
128. Stankovich S et al. *Nature* **442** 282 (2006)
129. Schedin F et al. *Nature Mater.* **6** 652 (2007)
130. Blake P et al., arXiv:0803.3031
131. Bunch J S et al. *Science* **315** 490 (2007)
132. Lusk M T, Carr L D *Phys. Rev. Lett.* **100** 175503 (2008)
133. Sevincli H, Topsakal M, Ciraci S, arXiv:0711.2414
134. Park C-H et al. *Nature Phys.* **4** 213 (2008)

PACS numbers: 72.80.Rj, **73.43.–f**, 81.05.Uw
DOI: 10.1070/PU2008v051n07ABEH006575

Electron transport in graphene

S V Morozov, K S Novoselov, A K Geim

1. Two-dimensional crystals

Carbon is an amazing chemical element that produces the most diverse structures. In addition to graphite and diamond, known since time immemorial, the attention of the scientific community is now focused on the recently discovered fullerenes [1–3] and nanotubes [4]. Unfortunately, experimenters could only work with three-dimensional (graphite, diamond), one-dimensional (nanotubes), and zero-dimensional (fullerenes) forms of carbon because all attempts to prepare specimens of two-dimensional carbon were unsuccessful until recently.

This mysterious two-dimensional form (planar hexagonal packing of carbon atoms) was called graphene and surprisingly happened to become perhaps the most studied among all carbon allotropes: indeed, graphene is the starting point for all calculations related to graphite, fullerenes, and nanotubes. At the same time, the numerous attempts to synthesize such two-dimensional crystals all failed, with only nanometer-scale crystallites obtained [5]. This was not surprising, however, in view of the prevailing opinion that truly two-dimensional crystals cannot exist [6–10] (in contrast to familiar quasi-two-dimensional systems). Indeed, graphene seeds should have a very high perimeter-to-surface-area ratio in the course of synthesis, which should facilitate transformation to other carbon allotropes.

This continued until 2004, when a group of researchers in Manchester and Chernogolovka employed a surprisingly simple and even naive approach to prepare graphene (Fig. 1), which made graphene one of the hottest topics in modern solid state physics [11, 12]. A separate plane (of monatomic thickness) was segregated from a three-dimensional graphite crystal using so-called micromechanical cleavage (graphite is a spectacularly lamellar material and can be treated as a stack of two-dimensional graphene crystals only weakly bonded to one another). Furthermore, two-dimensional crystals of other materials were also obtained by this technique [12], e.g., boron nitride, some dichalcogenides, and a high-temperature superconductor Bi–Sr–Ca–Cu–O. In fact, a new class of materials was born — two-dimensional crystals, stable in the free state.